UCRL-53688
Distribution Category UC-70

DISCLAIMER

UCRL--53688

DE87 002742

Post-Test Thermomechanical Calculations and Preliminary Data Analysis for the Spent Fuel Test—Climax

T. R. Butkovich

W. C. Patrick

Manuscript date: September 1985

LAWRENCE LIVERMORE NATIONAL LABORATORY
University of California • Livermore, California • 94550

Available from: National Technical Information Service • U.S. Department of Commerce
5285 Port Royal Road • Springfield, VA 22161 • A03 • (Microfiche A01)

Contents

Post-Test Thermomechanical Calculations and Preliminary Data Analysis for the Spent Fuel Test—Climax*

Abstract

The Spent Fuel Test—Climax (SFT—C) was conducted to evaluate the feasibility of retrievable deep geologic storage of commercially generated, spent nuclear-reactor fuel assemblies. Thermomechanical response of the SFT—C was calculated before the test began using the finite-element structural analysis code ADINA and its companion heat transfer code ADINAT. While we found that the level of agreement between measured and calculated rock displacements was quite good, we needed to revise certain aspects of the heat transfer calculation, material properties, and *in situ* stresses to incorporate information obtained during and after the heated phase of the test.

The post-test calculations reported here were performed using the best available input parameters, thermal and mechanical properties, and power levels that were directly measured or inferred from measurements made during the test. This report documents the results of these calculations and compares those results with selected measurements made during the 3-year heating phase and 6-month cooling phase of the SFT—C.

Introduction

A test of retrievable deep geologic storage of spent fuel assemblies from an operating commercial nuclear reactor was recently completed in a granitic intrusive at the U.S. Department of Energy's (DOE) Nevada Test Site (NTS). This project, called the Spent Fuel Test—Climax (SFT—C), is part of the Nevada Nuclear Waste Storage Investigations, which are managed by the Nevada Operations Office of the DOE. The Lawrence Livermore National Laboratory (LLNL) was responsible for the technical direction of the test (Ramspott et al., 1979), and is in the process of documentating the results of the SFT—C.

In addition to evaluating the feasibility of deep geologic storage, the test provided an excellent opportunity to study large-scale responses of a granitic rock mass to extensive heating and subsequent cooling to near ambient conditions. Specific test objectives related to the thermomechanical response of the rock mass were to:

- Evaluate our ability to numerically model the response of the rock mass to an episode of heating and subsequent cooling.
- Compare the response of sheared and fractured rock to the thermal load with the response of relatively unfractured rock.
- Compare the magnitude of displacement and stress effects from mining with those induced by extensive heating of the rock.

To accomplish these objectives, a series of calculations was undertaken using the ADINA structural analysis code (Bathe, 1978) and its companion heat flow code ADINAT (Bathe, 1977). These finite-element codes were chosen for their

* Prepared by Nevada Nuclear Waste Storage Investigations (NNWSI) Project participants as part of the Civilian Radioactive Waste Management Program. The NNWSI Project is managed by the Waste Management Project Office of the U.S. Department of Energy, Nevada Operations Office. NNWSI Project work is sponsored by the Office of Geologic Repositories of the DOE Office of Civilian Radioactive Waste Management.

ability to either directly or indirectly treat the phenomena of interest in the SFT—C, and because of their broad acceptance and ongoing development. Of particular importance were the coupling of heat flow and mechanical response, excavation sequencing, arbitrary stress boundary conditions, and a provision for simulating ventilation effects.

Scoping calculations of the effects of mining and thermal loadings provided a basis for selecting the types and locations of instrumentation to be used to monitor the response of the rock mass to excavation and heating (Butkovich, 1980). Since these calculations were completed before the test was under way, it was necessary to estimate input power histories of the spent fuel (Schmittroth et al., 1980), to use laboratory values for rock mechanical properties (Pratt et al., 1979), to estimate the *in situ* state of stress from the depth of the overburden, and to use planned spacings and dimensions of the underground openings.

By the time construction of the SFT—C was complete, a variety of new information was available for use in as-built calculations of the thermomechanical response of the rock mass (Butkovich, 1981). *In situ* stress measurements showed that the state of stress was anisotropic and spacially variable, and that the horizontal stresses exceeded the vertical (Ellis and Magner, 1982), contrary to the estimates used in the scoping calculations. In addition, field estimates of the deformability of the rock mass showed that the *in situ* modulus was substantially lower than laboratory values, and that a region of rock surrounding each underground opening was damaged by nearby detonation of explosives used to fragment the rock during the excavation (Heuze et al., 1981). Calorimetry measurements established that the actual power level of the spent fuel assemblies was somewhat lower than calculated by Schmittroth et al. (1980). Because of the variabilities and uncertainties in the various input data, the as-built calculations used a range of *in situ* moduli.

During construction of the SFT—C, an experiment known as the "Mine-By Test" was conducted. When major disagreements between calculated and measured stress changes and displacements were observed, several additional calculations were performed. Calculations by Schrauf and Board (1979) using the finite-element code TWODI and the boundary element code DIG produced results consistent with those of ADINA, and hence, inconsistent with the data. Because none of these calculations incorporated discrete geological features such as fractures and shear zones, Heuze et al. (1981) studied how such features would influence the response of the rock mass to the excavation process. Using the JPLAXD code, they found that although localized stress decreases occurred, the net effect was for mean vertical stress to increase with an attendant dilation of the pillar. The calculated stress changes were in good agreement with the field observations. However, the calculated displacements were within a factor of two of the measured displacements for only about 10% of the anchors, leading the authors of that report to speculate that the instruments may have malfunctioned. This discrepancy between measured and calculated responses to excavation is as yet unresolved and is not addressed further in this report.

This report has two purposes. First, we are documenting our attempts to improve upon the design calculations by incorporating refinements in the material properties, *in situ* stresses, and thermal sources. In addition, we drive the mechanical portion of the calculation with nodal point thermal histories that closely approximate the multipoint thermal measurements. Second, we present and analyze selected rock mass displacements and stresses in the context of these calculations.

Test Description and Geometry

Location and Configuration

The SFT—C is located 420 m below the ground surface in the quartz monzonite unit of a two-part intrusive known as the Climax stock. At the test level, the rock is about 150 m above the regional water table and is unsaturated but not dry. Wilder and Yow (1984) report four dominant joint sets and three much less prominent sets in the test area. The dominant sets may be described by orientations of N44W-22NE, N24W-vertical, N59W-vertical, and N48E-80SE. As a result of the dominant sets, the rock mass is moderately jointed with frequencies ranging from 0.9 to 2.2 joints/m.

The basic configuration of the test is shown in Fig. 1. The three parallel drifts, spaced about 10 m

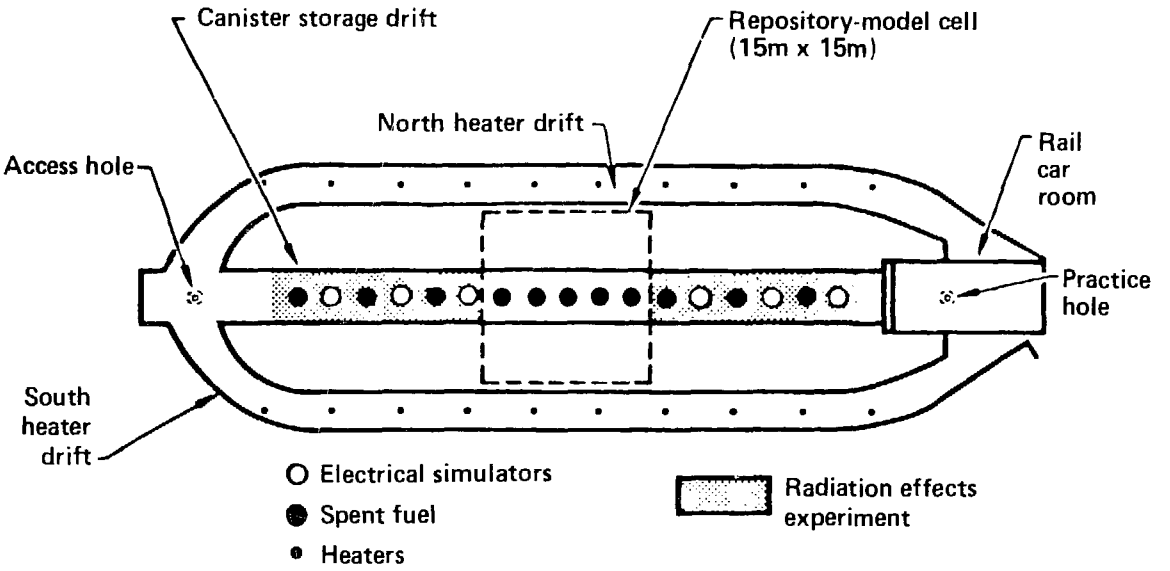

Figure 1. Plan view of the SFT—C showing the location of spent fuel and related heat sources.

on centers, were excavated in three steps. The two 3.4- by 3.4-m cross-section heater drifts were excavated first, essentially in parallel. When the excavation of the heater drifts was complete, the upper 3.5 m of the canister drift was excavated. Then the bench was excavated to produce the 6-m-high by 4.6-m-wide drift. This three-step excavation sequence is treated explicitly in the thermomechanical calculations.

Eleven canisters containing single, intact spent-fuel assemblies aged about 2.5 years out of core (YOC)* were emplaced in 0.61-m-diameter by 6-m-deep boreholes drilled in the floor of the central drift. The spent-fuel assemblies were interspersed with six electrically heated simulators located in boreholes of the same size and geometry. To simulate the thermal field of a large repository, 10 auxiliary electrical heaters were located in boreholes spaced 6 m apart in the floor of each of the two side drifts. Because the ADINA/ADINAT calculations model a unit thickness of the SFT—C array, the spent-fuel assemblies, electrical simulators, and auxiliary heaters were modeled as strip sources with their actual powers distributed according to the dimensions of the unit cell used in the calculations.

Instrumentation

Temperatures, displacements, and stress changes were measured during the 3-year heating phase and subsequent 6-month cooling phase of the SFT—C. Although the deposition and removal of thermal energy and the concomitant changes in the rock mass temperature constitute the driving force, the displacements and stress changes are of direct concern in this report.

We determined the energy deposition history from each of the various sources using one of several means. First, the power history of the spent-fuel assemblies was determined from calculations and the results of calorimetry (Schmittroth et al., 1980). Second, using electronic control systems, the power histories of the electrical simulators were made to match those of the spent-fuel assemblies. Third, the thermal output of the auxiliary heaters was controlled and measured by Watt transducers, as were the incidental sources of energy such as facility lighting (Brough and Patrick, 1982).

Thermocouples were placed throughout the test array to measure the distribution of temperatures during the test (Brough and Patrick, 1982). Although they were mostly concentrated close to canisters (Fig. 2), they were also placed so as to measure temperatures relatively far from the heat sources (Fig. 3). Of particular interest here are those thermocouples located on or adjacent to instruments that measured displacements or stress

* All times are based on the spent fuel age in years out of core (YOC). The spent fuel was 2.46 YOC at the start of testing.

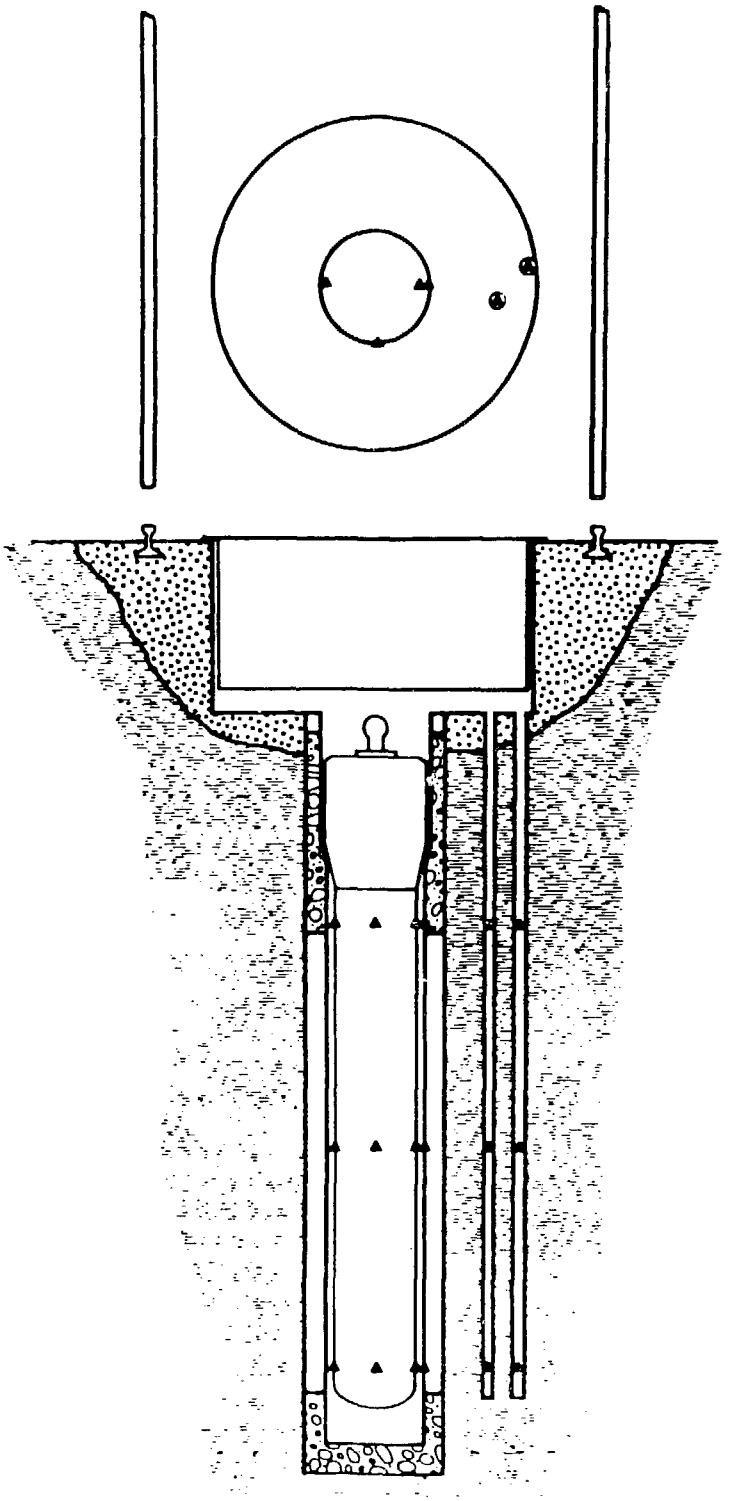

Figure 2. Near-field thermocouple locations are designated with triangles.

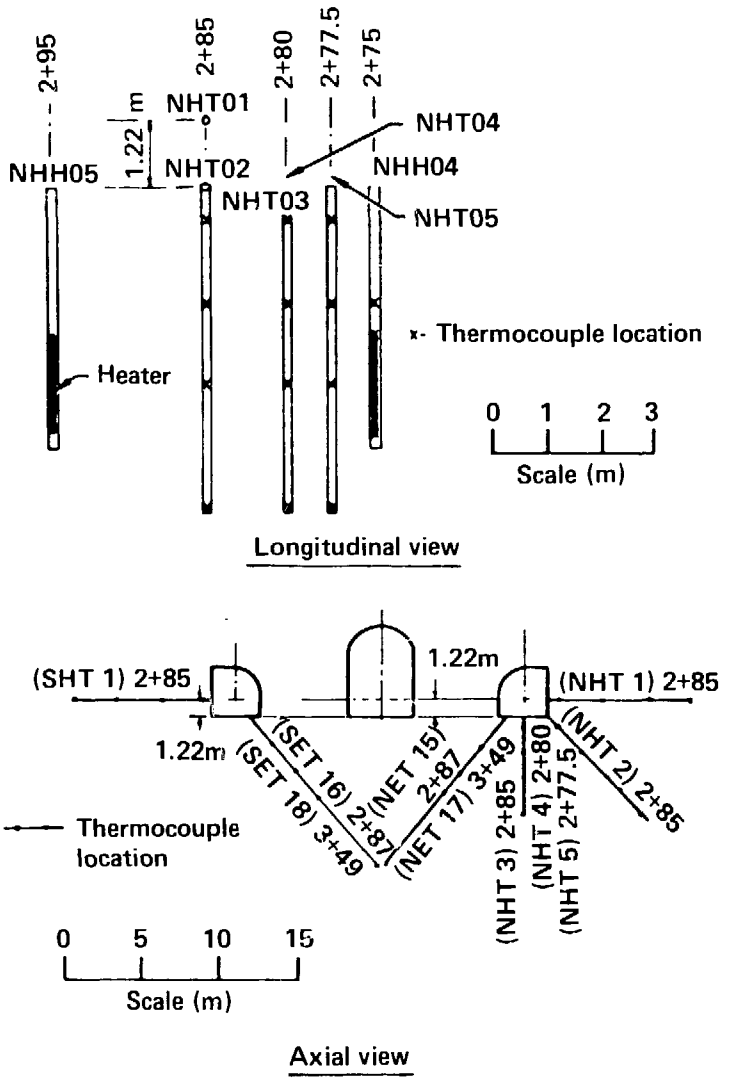

Figure 3. Intermediate- and far-field thermocouple locations in the storage facility are indicated by dots.

changes (Figs. 4a and b). These sensors fulfilled the dual roles of providing a basis for compensating for the effects of thermal expansion of instrument components and recording the temperature distribution for comparison with ADINAT calculations.

We also monitored the characteristics of the ventilation air stream. The "dry bulb" temperatures and dewpoints of the inlet and outlet airstreams, together with air flow rates, were used to determine the quantity of energy removed by the ventilation system as a function of time (Fig. 5). Thus, the rate of energy removal from the SFT—C is known.

Geomechanical instrumentation was located throughout the SFT—C to monitor the displacements and stress changes that occurred as the rock mass was initially excavated, heated, and cooled. Multipoint borehole extensometers (MPBX) were installed in three orientations at four different locations in the pillars between the heater drifts and the canister drift (Fig. 4). Whereas the 4 horizontally oriented units had 3 anchor points, the units oriented at 34 and 50 degrees above horizontal

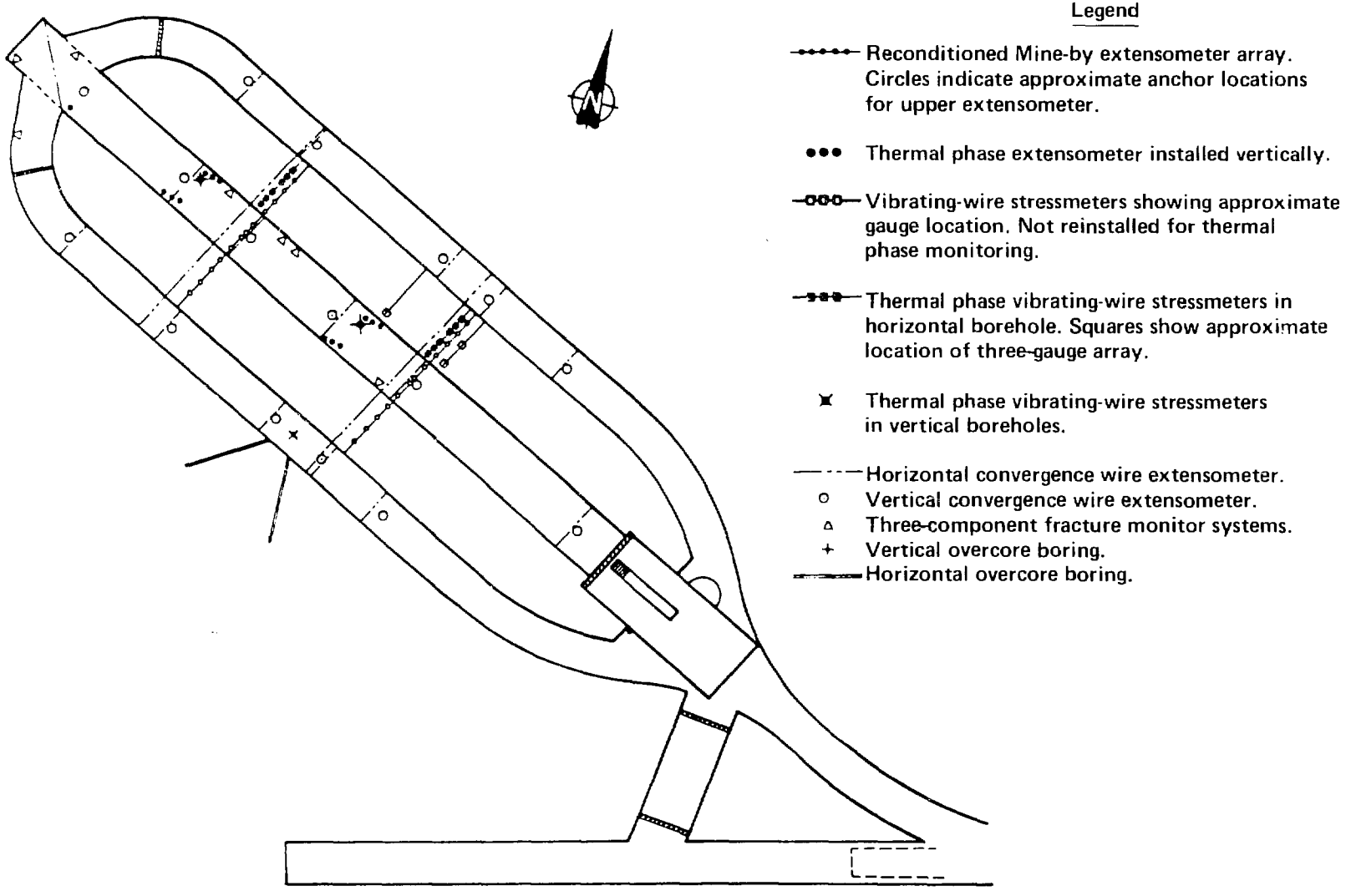

Figure 4a. Location of thermal phase instrumentation.

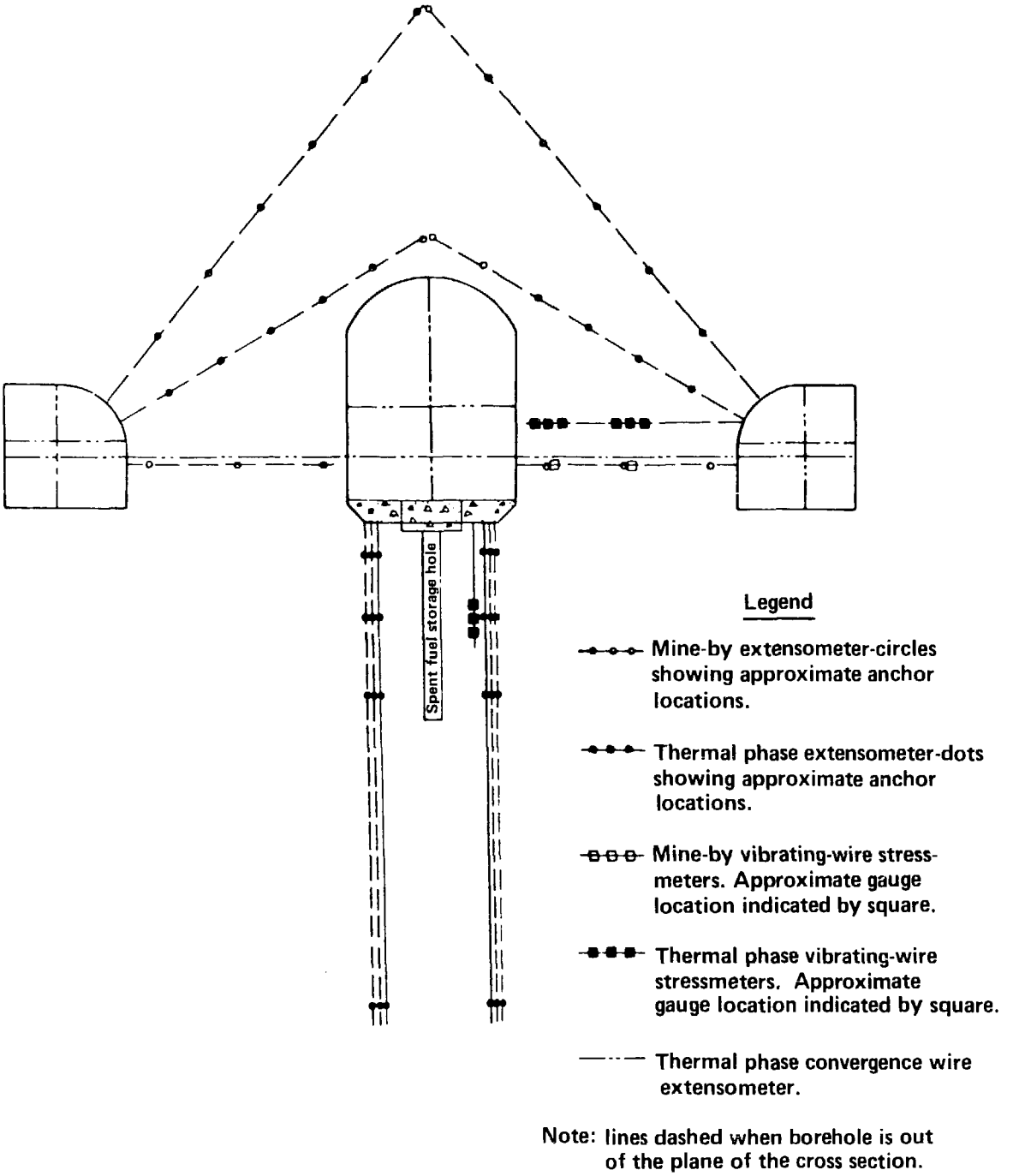

Figure 4b. Cross section showing thermal-phase and Mine-By instrumentation arrays.

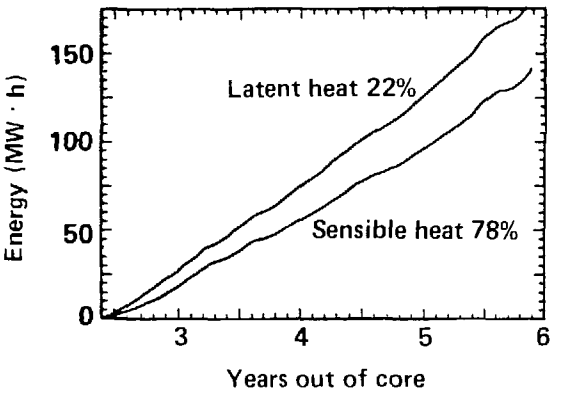

Figure 5. Cumulative thermal energy removed by ventilation.

each had 6 anchor points. These units, called Mine-By instruments (MBI), were installed to record displacements that occurred during the Mine-By experiment, and were refurbished for continued use during the heating and cooling phases of the test (Brough and Patrick, 1981). After excavation, 14 four-anchor MPBX units were installed in the floor of the canister drift to measure displacements within the rock mass during the heated phase of testing (Figs. 4a and b).

We installed 16 orthogonal sets of convergence wire extensometers (CWE) to measure displacements within the drifts. These units measured the relative displacements between the roof and the floor and between opposing walls of the drifts. Each CWE was outfitted to permit parallel tape extensometer measurements to be made (Figs. 4a and b).

One of the objectives of the geotechnical measurements program was to examine the relative contribution of movements along geological discontinuities to the total "elastic" response of the rock mass. Seven three-component fracture monitor systems (FMS) were deployed at selected locations to obtain these measurements. Since the ADINA thermomechanical response calculations reported here do not explicitly treat the presence of such features, the results of these measurements will be discussed in another report that is currently being prepared.

Changes in the state of stress were monitored at selected locations using IRAD-vibrating-wire stressmeters. A total of 18 units were installed as rosettes of three, 1 m radially outward from each of 2 spent-fuel assemblies, and at pillar center and 0.7 m in from the canister drift at each of 2 locations in the north pillar (Figs. 4a and b).

As described by Patrick, Carlson, and Rector (1981) and by Patrick, Rector, and Scarafiotti (1984), several of the geomechanical instruments malfunctioned during the heated phase of the SFT-C. As a result, not all instruments provided continuous data records. The most critical data losses were from the vibrating-wire stressmeters and the vertical MPBX units located in the floor of the canister drift. Interpretation of data from these sources is presented in the report in preparation noted above.

Energy Deposition and Removal

At the time the design calculations were completed from the SFT—C, the precise power histories of the spent fuel, electrical simulators, and auxiliary heaters were not known. The same is true with regard to variations in the ventilation flow rate and the inlet air-stream temperature history. However, test measurements provided better estimates of the energy deposition and removal rates for use in the post-test calculations reported here.

The total contribution of each energy source is shown in Table 1, and the contributions as a function of time are shown in Fig. 6. Because of the relatively minor contribution of the facility lighting to the total energy deposition, this source was not treated explicitly in any of the calculations and is not discussed further.

Our current understanding of the power history of the spent fuel is as indicated in Fig. 7. In this figure, the power table developed by Schmittroth et al. (1980) has been adjusted to bring it into better agreement with calorimetry data obtained early in the test.

Figure 7 also shows the power history of the electrical simulators as measured by watt transducers. In general, the stair-step of the adjustments to the simulator power levels closely matches the decay curve of the spent fuel. Before 3.1 YOC, the simulator power levels were consistently above the decay curve because the original decay curve, unadjusted for calorimetry results, was somewhat higher than the present curve. The resulting error is an insignificant portion of the more than 1 GW·h of energy deposited during the test.

At the beginning of the test, the spent-fuel assemblies were emplaced and the simulators were energized during a 6-week period beginning April 18, 1980, and ending May 28, 1980. Likewise, at the end of the heating phase of the test they

Table 1. Cumulative energy input to the SFT—C by source.

Source	Cumulative energy through fuel retrieval		Cumulative energy through cool-down	
	MW·h	% of total	MW·h	% of total
PWR fuel assemblies (11)	263.4	25.3	263.4	24.8
Electrical simulators (6)	148.0	14.2	148.0	14.0
Guard heaters (20)	600.6	57.7	600.0	56.7
Facility lights	29.0	2.8	48.0	4.5
Totals	1041.0	100.0	1060.0	100.0

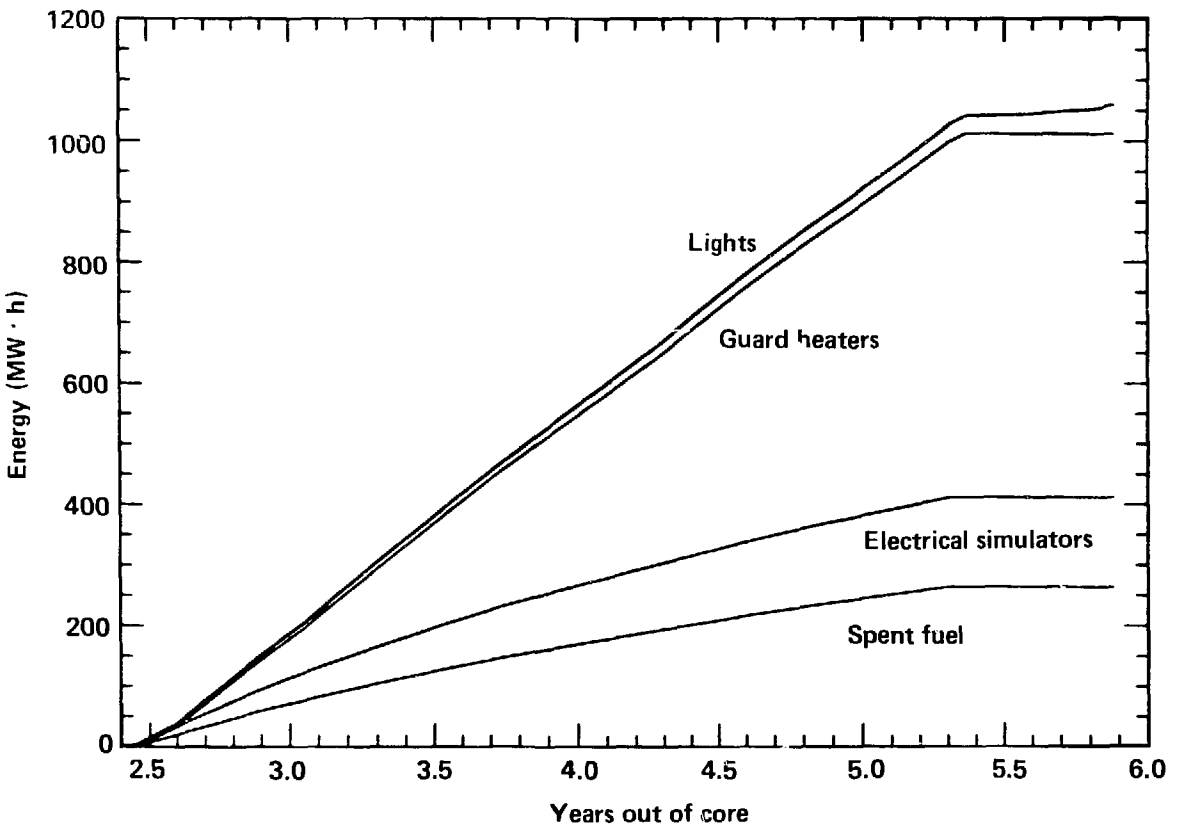

Figure 6. Cumulative thermal energy input by source.

were retrieved or de-energized as appropriate between March 3, 1983, and April 6, 1983. Because we modeled the facility as an infinite-length array using a unit cell approach, these heat sources could not be individually treated in the calculations. Instead, the calculations began to deposit energy at a time corresponding to the insertion of the central spent-fuel assembly (May 8, 1980), and stopped when this assembly was removed (March 24, 1983).

The power levels of the auxiliary heaters are shown in Table 2. To simulate the thermal conditions of a panel of a large-scale repository, the power levels of these sources increased as the test progressed. The stepwise increase in power closely approximated the thermal pulse generated

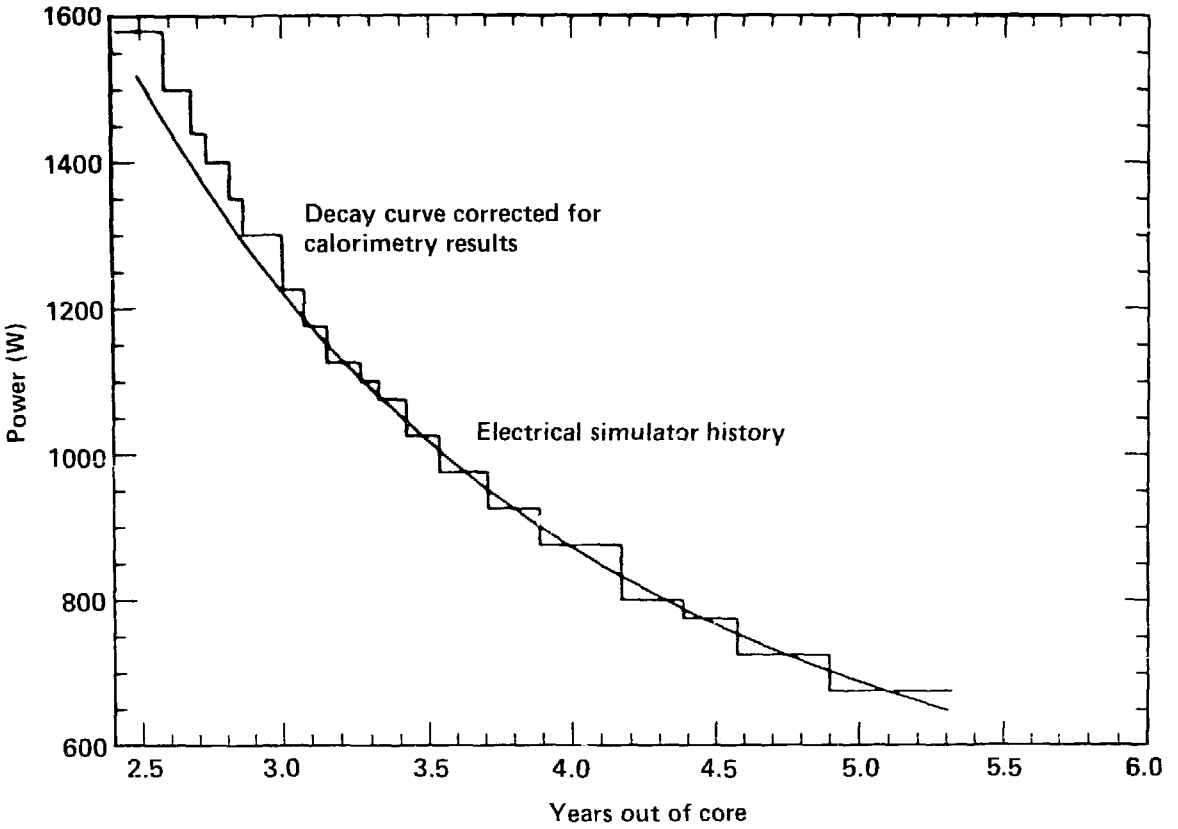

Figure 7. PWR fuel assembly and electrical simulator power history.

Table 2. Auxiliary heater power history.

Date of change	Power (W)	Comments
May 8, 1980	0	Start of test
June 27, 1980	1850	Too high
July 2, 1980	925	Target
December 16, 1980	1250	Target
February 19, 1982	925	Too low
March 1, 1982	1400	Compensating value
April 8, 1982	1350	Target

by the interaction of many parallel rows of heat sources in a large repository, as shown by Montan and Patrick (1981). Since the auxiliary heaters were simultaneously energized and de-energized, the timing of their energy deposition is treated explicitly in the thermomechanical calculations.

By measuring the characteristics of the inlet and exhaust air stream, the removal of energy from the SFT—C was carefully monitored. Because the ADINAT heat flow calculations were not designed to evaluate our ability to model thermal energy removal in the ventilation air stream, we took the liberty in these post-test calculations to use the measured energy removal rate data as a thermal sink rather than attempt to revise the "pseudoproperties" that were used in the design calculations to simulate the ventilation process (Butkovich and Montan, 1980; Butkovich, 1981). While this approach does not constitute a direct modeling of the ventilation process, it allows us to obtain a better level of agreement between measured and calculated rock temperatures and hence, limits the influence of discrepancies in rock temperature on the thermomechanical response of the rock mass.

Heat Transfer Calculations and Comparisons with Data

General Considerations and Input Data

The thermal calculations were carried out using the ADINAT finite-element code, which is compatible with the ADINA displacement and stress analysis code. ADINAT produces nodal point thermal histories that drive the thermomechanical ADINA calculations.

Correctly modeling heat transfer in the SFT—C required a heat transfer code with conduction, radiation, and ventilation capabilities. In addition to conductive heat flow through the rock mass, radiative heat transfers occurred between the floor, walls, and roof of the drifts. Furthermore, heat was removed by the ventilation air stream passing through the drifts. However, the present version of the ADINAT code allows radiative heat transfer only from the external boundary of the calculational mesh, and heat transfer to the ventilation air is not directly modeled. Butkovich and Montan (1980) devised a method that enables ADINAT to model internal radiative heat transport and ventilation. Radiation was modeled by assigning a high value of thermal conductivity and a low mass density to the material that constitutes the openings. To simulate ventilation, we first connected all side nodes in each drift to a central node. This node was then connected to an outside point with a fixed temperature. A temperature-dependent convective heat transfer coefficient controlled heat transfer between this outside point and the central node.

For the "as-built" calculations, the values of thermal conductivity of the drift material and convection coefficient were varied until the temperatures of selected nodes closely matched the results from a TRUMP code calculation. TRUMP (Edwards, 1972) correctly models radiative heat transport between drift surfaces as well as conductive and convective thermal transport to and through the air in the drifts, and includes energy removal in the ventilation air stream. The meshes of the ADINAT and TRUMP calculations were made as similar as possible so the results could be compared.

When the temperature data became available, it showed that the calculated and measured results differed by as much as five degrees, particularly in the regions near the surfaces of the underground openings. Since the purpose of the ADINAT thermal calculation was to produce the correct temperature change with which the thermomechanical calculation would be driven, the convection coefficient that controls the rate of removal of heat by the ventilation air stream was varied until good agreement between measured and calculated temperatures was obtained.

The finite-element mesh constructed for the as-built calculations was also used for the post-test calculations reported here (Fig. 8). Since there is approximate symmetry with respect to the vertical center line through the spent-fuel drift, only half of the planar cross section is modeled. In constructing the mesh, we provided for a 0.5-m-wide element group surrounding the excavations so that a region around each opening that was damaged by explosives in the mining process could be assigned different properties than the rest of the rock mass. With the exception of the degenerated four-node elements used for the material removed in the excavation, all of the elements consisted of eight nodes. Table 3 shows the distances and spacings used in the construction of the finite element mesh.

Table 4 shows the thermal properties of the Climax stock quartz monzonite used in the ADINAT calculations. The power input to the spent-fuel canisters and electrical simulators is that shown as the solid curve in Fig. 7. The auxiliary heater power history is shown in Table 2.

Comparisons Between Calculations and Data

The convection coefficients (which control heat transfer out of the mesh) were varied until a good fit to all of the temperature data measured throughout the entire heating and cooling portions of the test was produced. Figures 9a–d show typical temperature-time curves for selected positions around the openings, comparing measured and calculated results. The data are represented by 9.13-day averages of measurements that were made several times each day. The 9.13-day period corresponds to the time step length in the ADINAT/ADINA calculations (40 time steps per year). The temperature of each nodal point throughout the mesh at the start of the calculation was 23.5°C, whereas the measured temperatures were within about one degree of this average value.

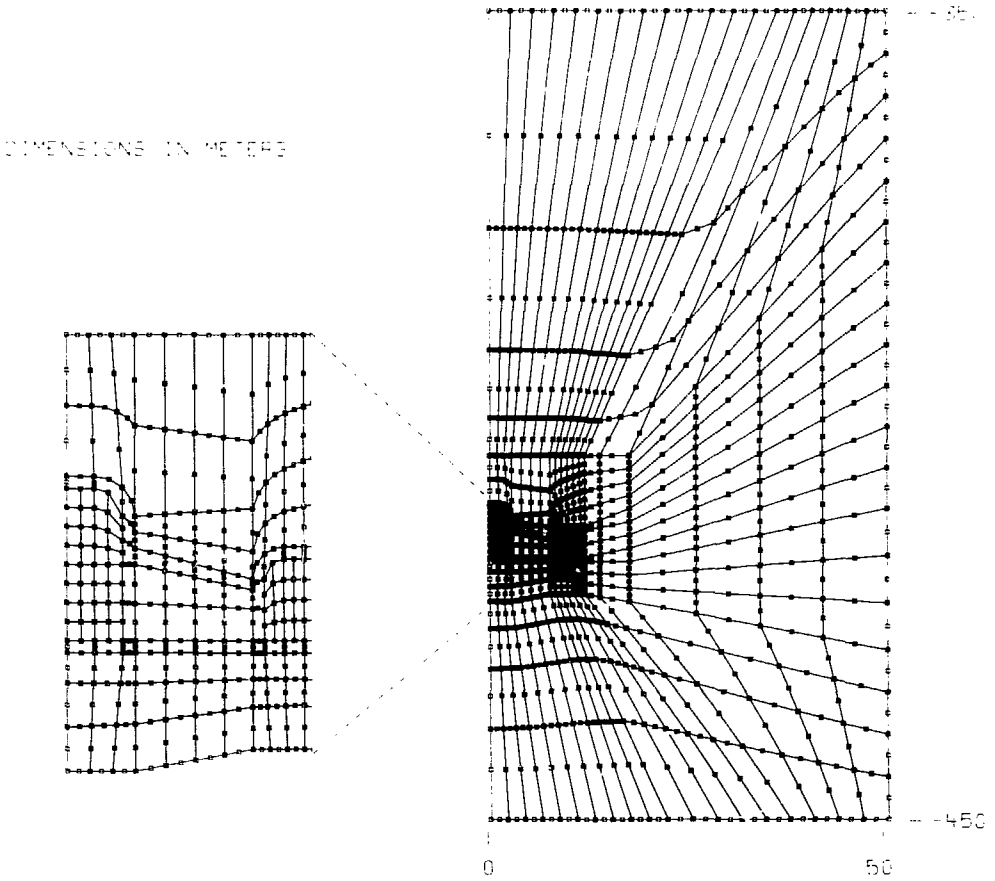

Figure 8. Finite-element mesh used in ADINAT/ADINA calculations.

Table 3. Distances and dimensions used in ADINA/ADINAT calculations.

Spent fuel	Distance and dimensions
Floor position	417.58 m below surface
	1.75 m above top of canister
Cross section	4.58 × 6.25 m with domed roof
Heater drift	
Floor position	417.58 m below surface
	3.35 m above top of heater
Cross section	3.35 × 3.35 m with rounded corner
Spent fuel canisters and electrical simulators	
Spacing	3 m on center
Length	3.66 m
Electrical resistance heaters	
Spacing	6 m on center
Length	1.83 m

Table 4. Thermal properties of Climax stock granite used in the calculations.

Heat capacity[a]	930 J/kg·K
Thermal conductivity (°C)[b,c]	
0	3.1679 W/m·K
27	3.1104
477	2.1104
Thermal expansion coefficient (°C)[d]	
0	10×10^{-6}/K
23	10
40	8.9
80	7.4
125	8.0
175	9.6
225	12.7

[a] Derived from diffusivity measurements.

[b] Pratt et al. (1979).

[c] Montan and Bradkin (1984), determined the *in situ* conductivity at the test level for temperatures of ~23 to ~95°C to be 3.1 W/m·K.

[d] Heard (1980), values based on measurements at effective pressure of 13.8 MPa.

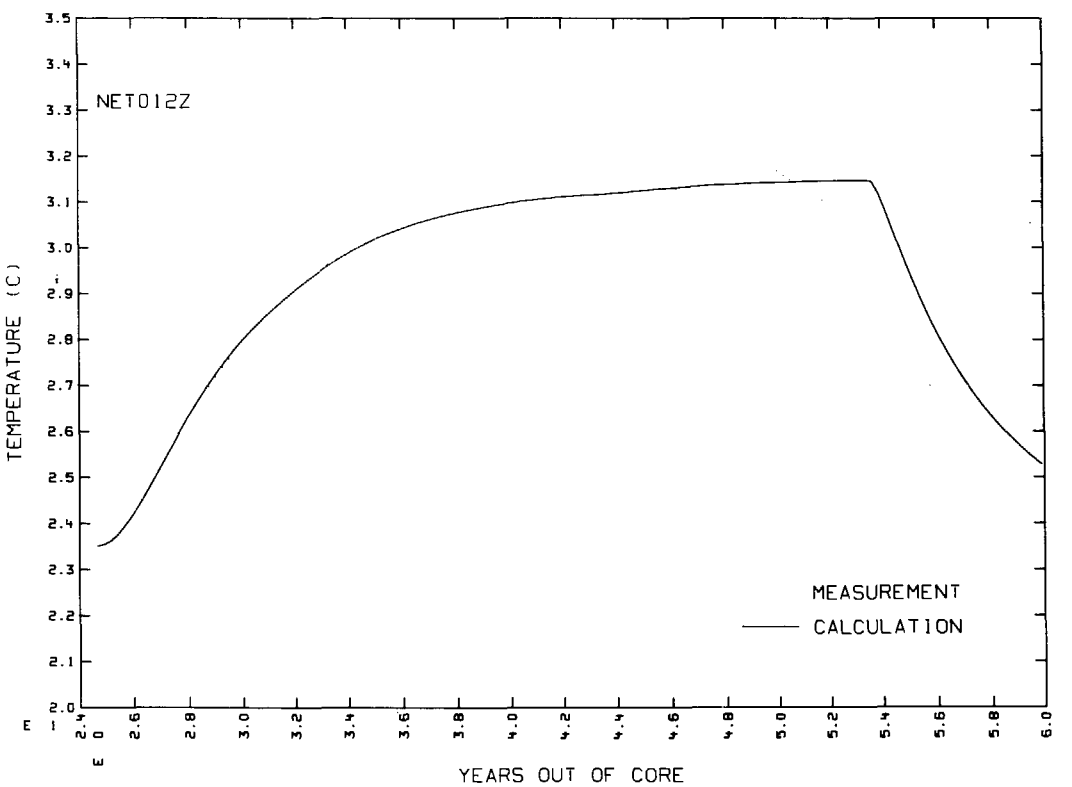

Figure 9a. Nodal point temperature history for a point in mid-rib intersected by horizontal extensometer compared with nearby measured values.

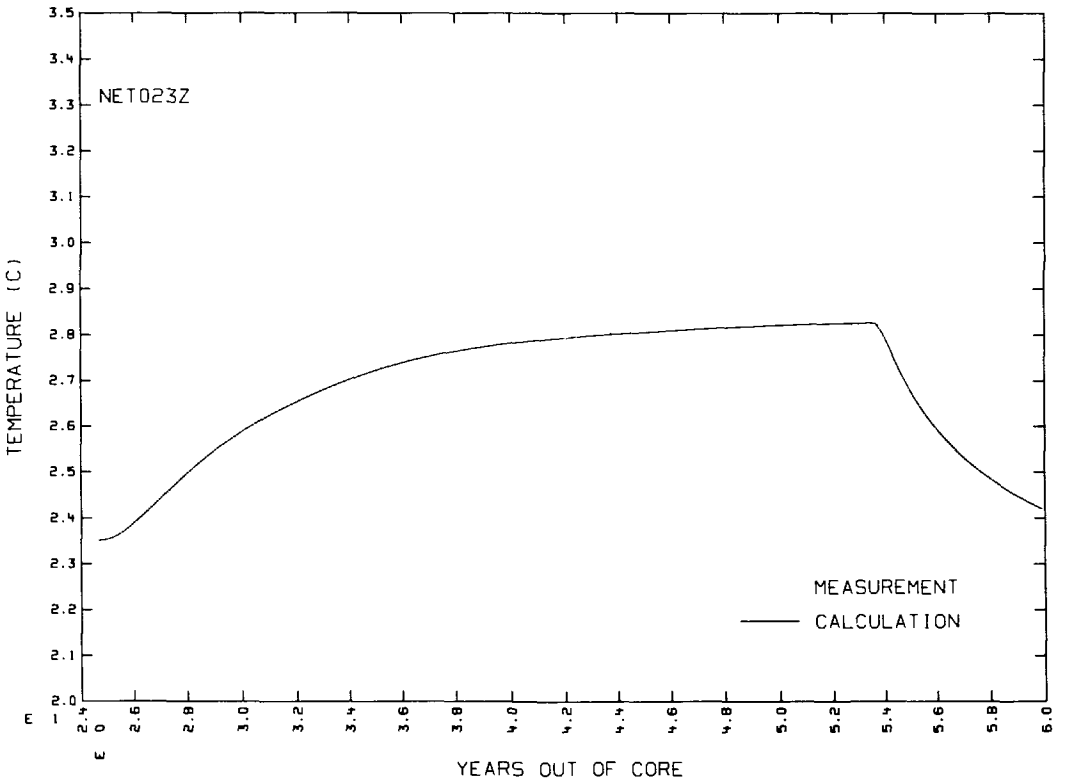

Figure 9b. Nodal point temperature history for a point in mid-rib intersected by 34° extensometer compared with nearby measured values.

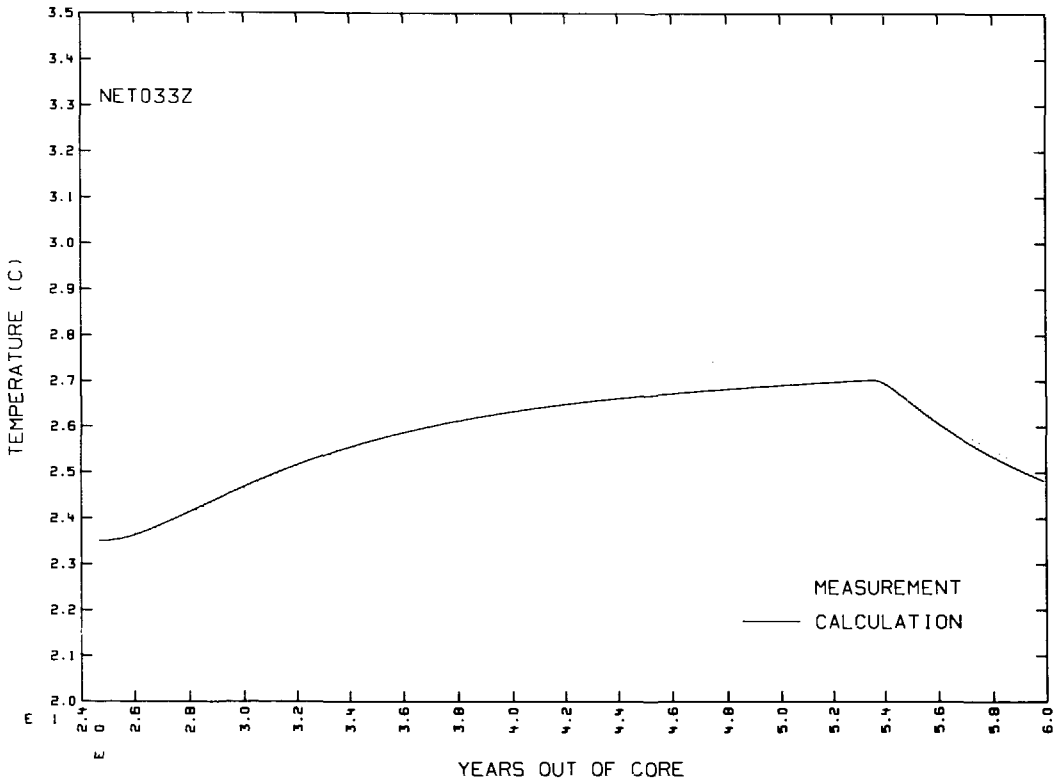

Figure 9c. Nodal point temperature history for a point in mid-rib intersected by 50° extensometer compared with nearby measured values.

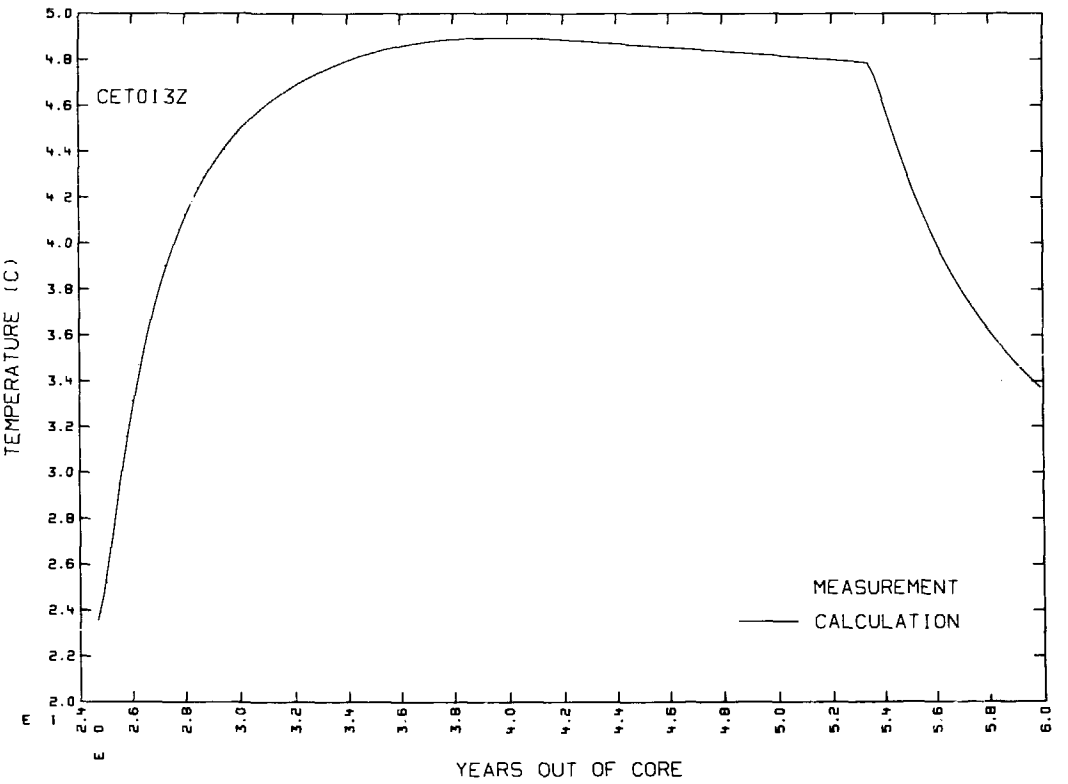

Figure 9d. Nodal point temperature history for a point near spent-fuel canister compared with nearby measured values.

Figures 10a-d compare the measured and calculated values of temperature change from the start of the test for 27 locations above and below the openings at station 2 + 83, near the center of the test facility. The times chosen for the comparisons correspond to spent-fuel ages of 3.0, 4.0, and 5.0 YOC, as well as the end of the test. If the calculation and measurements agreed exactly, all the points would fall on the line with slope = 1 and y-intercept = 0. The figures also show the slope (A1) and y-intercept (A0) of the best-fit straight line and the root-mean-square errors (RM). In all cases, we see R^2 (RR) values of at least 0.98 and root-mean-square errors of less than 1°C. These compare favorably with the ISA special limits of error for thermocouples (1.1°C) and with the individual calibrations (Patrick, Rector, and Scarafiotti, 1984). This is an exceptionally good level of agreement when one considers that the positions of the temperature measurement points are not coincident with nodal points in the finite-element mesh for which the calculated temperatures are shown. Around the rib where the elements are smaller, the nodal points are within 0.25 m of a measurement point. For regions away from the openings where the mesh is more coarse, the nodal points may be as much as 1.0 m away from associated measurement points.

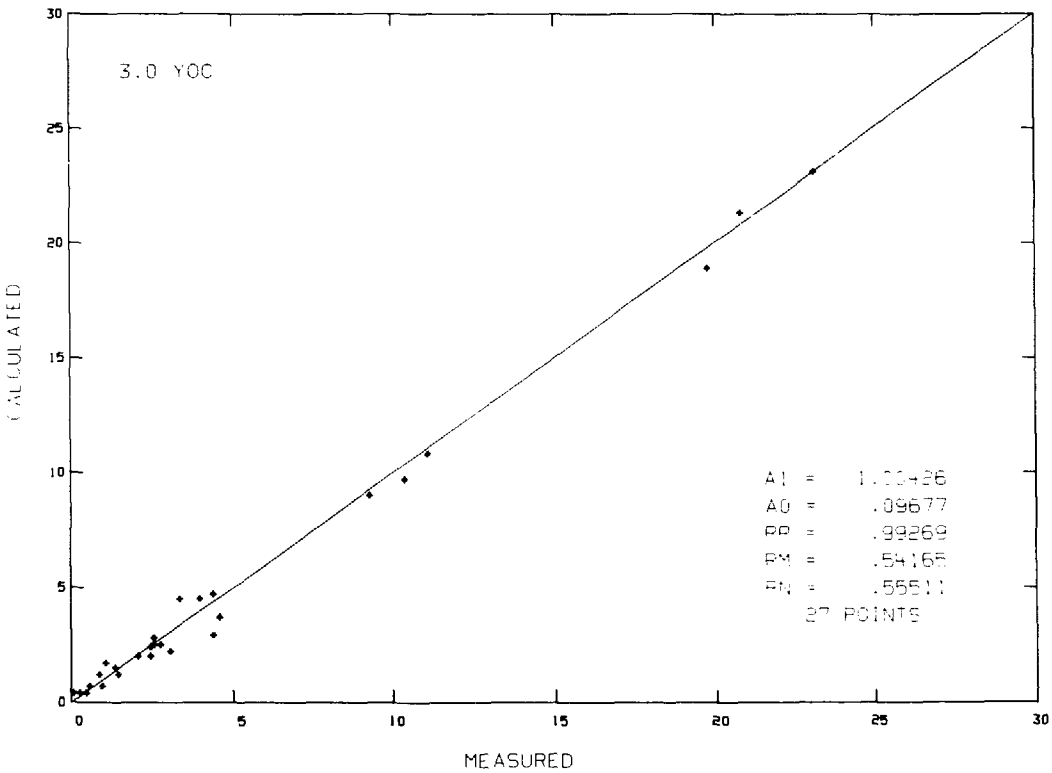

Figure 10a. Comparison of measured and calculated change in degrees Celsius for Station 2 + 83 at 3 YOC.

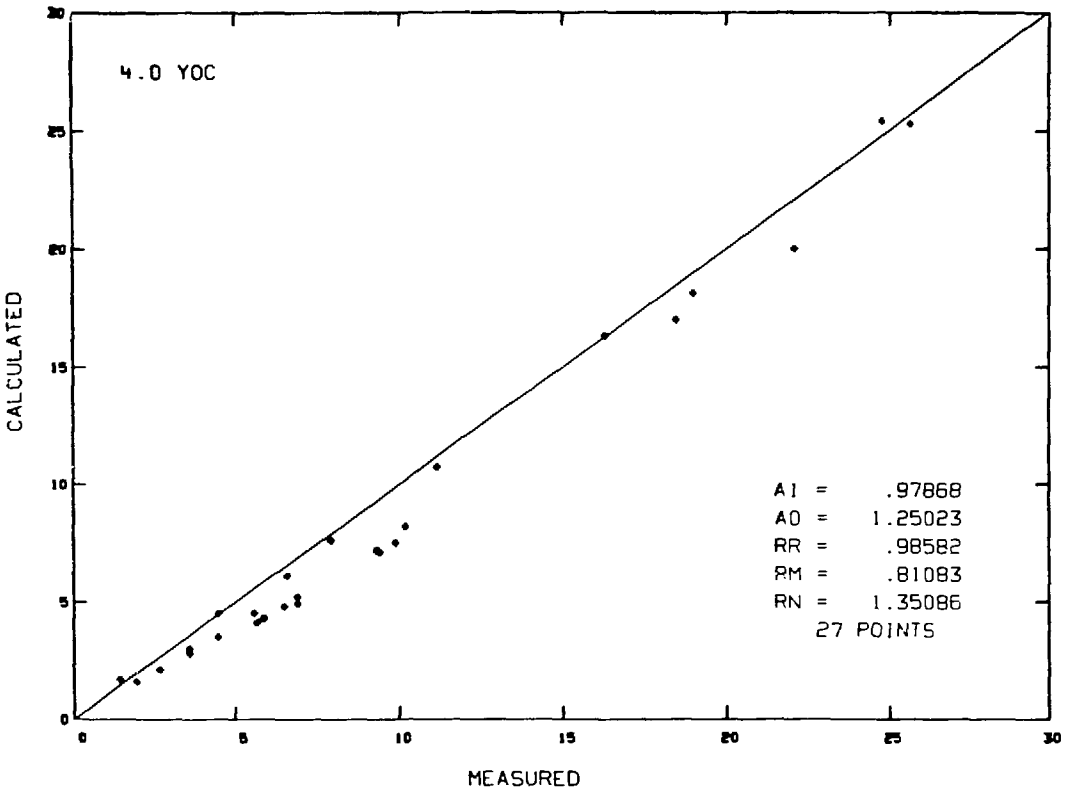

Figure 10b. Comparison of measured and calculated temperature change in degrees Celsius for Station 2 + 83 at 4 YOC.

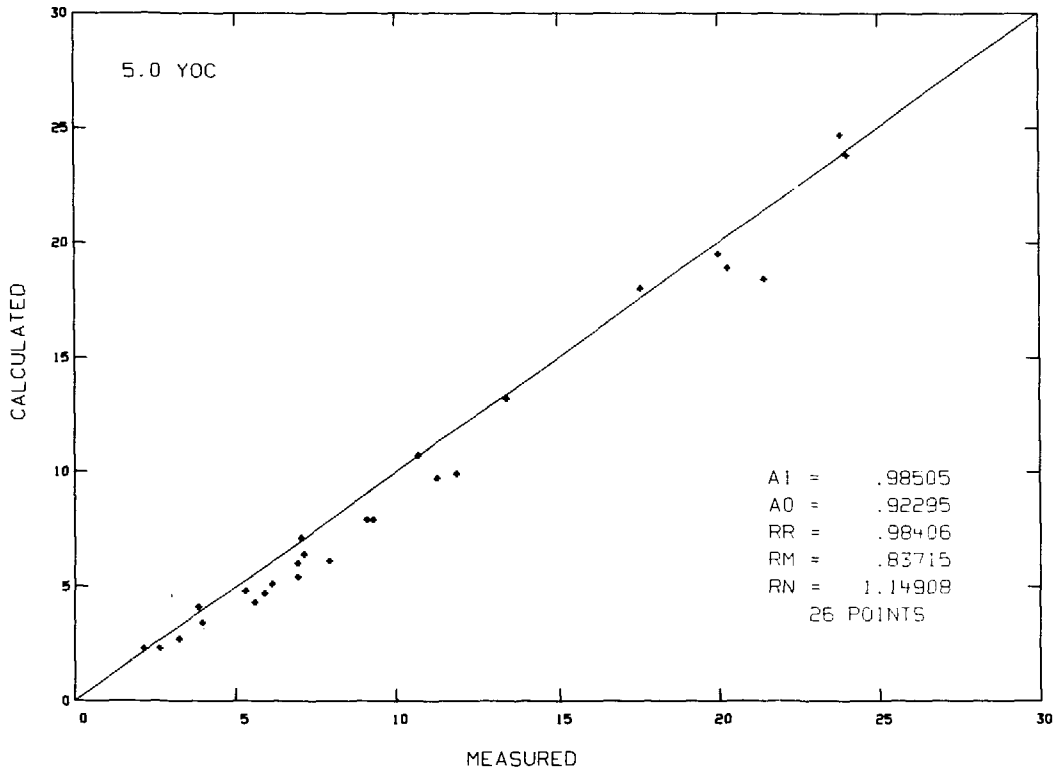

Figure 10c. Comparison of measured and calculated temperature change in degrees Celsius for Station 2 + 83 at 5 YOC.

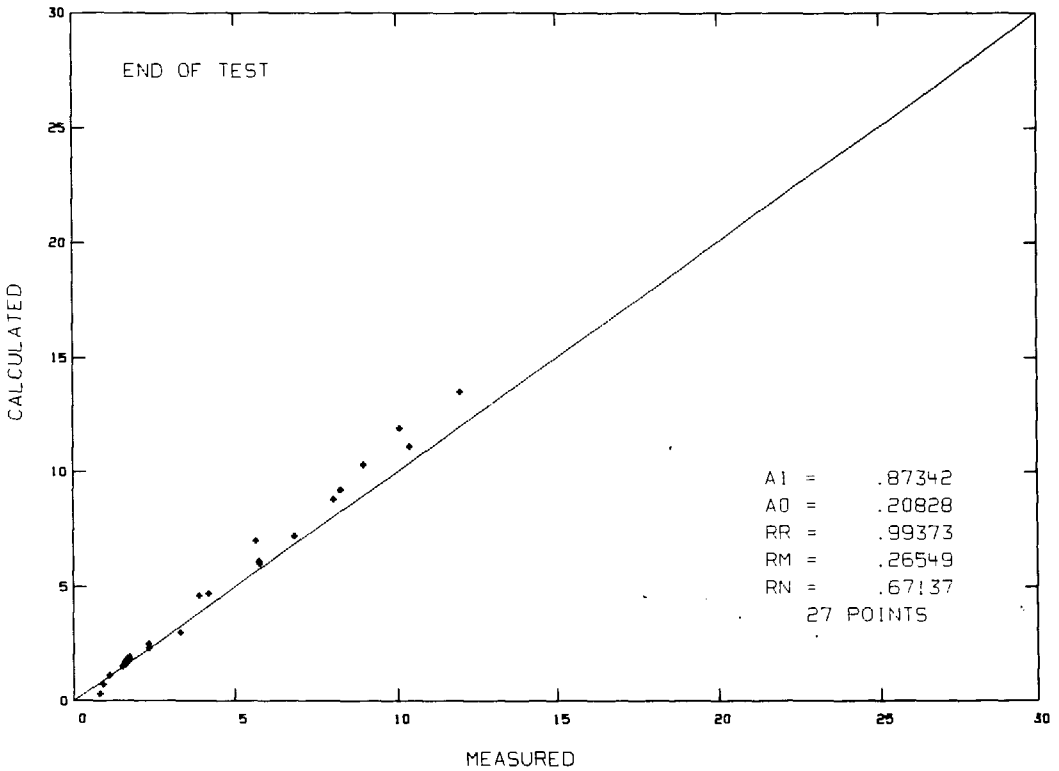

Figure 10d. Comparison of measured and calculated temperature change in degrees Celsius for Station 2 + 83 at end of test.

Thermomechanical Response Calculations and Comparisons with Data

General Considerations and Input Data

Initially, *in situ* stress data were obtained by Ellis and Magner (1982) in a set of relatively short boreholes drilled about 6 m outward from the south heater drift. At the time these measurements were made, excavation of the canister drift was just beginning. Presumably the effect of the canister drift excavation on these values was minimal. The principal stresses measured by Ellis and Magner (1982) were rotated into the plane of the calculation and used in boundary loadings to the finite-element mesh in the as-built calculations (Butkovich, 1981). The resulting shear stresses were ignored. After the heating phase of SFT—C was completed, Creveling et al. (1984) performed an extensive suite of stress measurements using two independent techniques in boreholes up to 30 m long. The measurements exhibited a high degree of spacial variability both in magnitude and in orientation. Possible sources of these variations are still under study. Given this variability, we performed several thermomechanical calculations using the range of values observed.

In situ deformability data were developed by Heuze et al. (1981) for use in calculations of excavation response with a discrete joint element code (Heuze et al., 1982). These data were also used in the as-built thermomechanical calculations (Butkovich, 1981). Patrick, Yow, and Axelrod (1985) recently completed deformation modulus measurements following the heated phase of the SFT—C. Their analyses of these data show:

- The mean deformation modulus is 37.7 GPa with 80% of the data values in the interval 12 to 63 GPa.
- The modulus of moderately fractured rock 2 m or more from excavated surfaces ranges from 40 to 55 GPa, based on post-heating measurements.
- The modulus of faulted, sheared, or intensely jointed rock ranges from 5 to 20 GPa.
- The rock modulus within 2 m of excavated surfaces ranges from 10 to 45 GPa.
- The modulus of the rock near the canisters and auxiliary heaters that was heated to temperatures in excess of 60° C ranges from 5 to 25 GPa.

After examining the available *in situ* stress and deformation moduli data, it seemed unreasonable to do calculations for all the possible combinations within the range of measurements. Furthermore, it was not possible to directly model the variability. Instead, we made three thermomechanical calculations using our best estimate of the moduli and stresses and extreme conditions on either side of this estimate. Each of these calculations used the same nodal point temperature histories obtained with ADINAT, as well as the temperature-dependent thermal expansion coefficients shown in Table 4. The thermal expansion coefficients used were taken from Heard (1979), who measured the expansion coefficients on samples of SFT—C quartz monzonite at confining pressures of 0, 13.6, and 27.8 MPa. Heard's results show that the thermal expansion coefficients decrease about 20% between 0 and 27.8 MPa confining pressure. The intermediate set of values was used as more representative, based on the measured *in situ* stress at test level. The values of input parameters for the three calculations are shown in Table 5.

Comparisons Between Calculations and Data

Results of the three calculations are shown for stress changes, tunnel closure, and relative displacements within the rock mass around the openings. When comparisons with measurements are shown, stress differences between two times are used. Tunnel closures are adjusted to agree with a calculation as of the start of the measurement period (several weeks after the start of heating) and are compared with the calculation from then until the end of the test. Relative displacement differences are compared at selected times during the test.

Stress Changes

The three points for which stress vs time results are shown coincide with the positions of the stress gauges. Figures 11a and b show the calculated horizontal and vertical stress vs time for a point mid-height in the pillar, 3 m from the heater drift. Figures 12a and b show similar results for a point mid-height in the pillar, 0.7 m from the

Table 5. **Elastic properties and mesh loadings used for three thermomechanical calculations.**

Property or parameter	Calculation number 1	2	3
Rock mass modulus	27 GPa	38 GPa	38 GPa
Rock mass Poisson's ratio	0.25	0.25	0.25
Damaged zone modules	13 GPa	19 GPa	19 GPa
Damaged zone Poisson's ratio	0.35	0.35	0.35
Vertical mesh loading[a]	6.21 MPa	6.21 MPa	12.60 MPa
Horizontal to vertical stress ratio	1.2	1.2	0.98

[a] Vertical mesh loading on *in situ* stresses measured at mid-rib. A value of 7.89 MPa was used in calculations 1 and 2 and a value of 14.28 MPa was used in calculation 3.

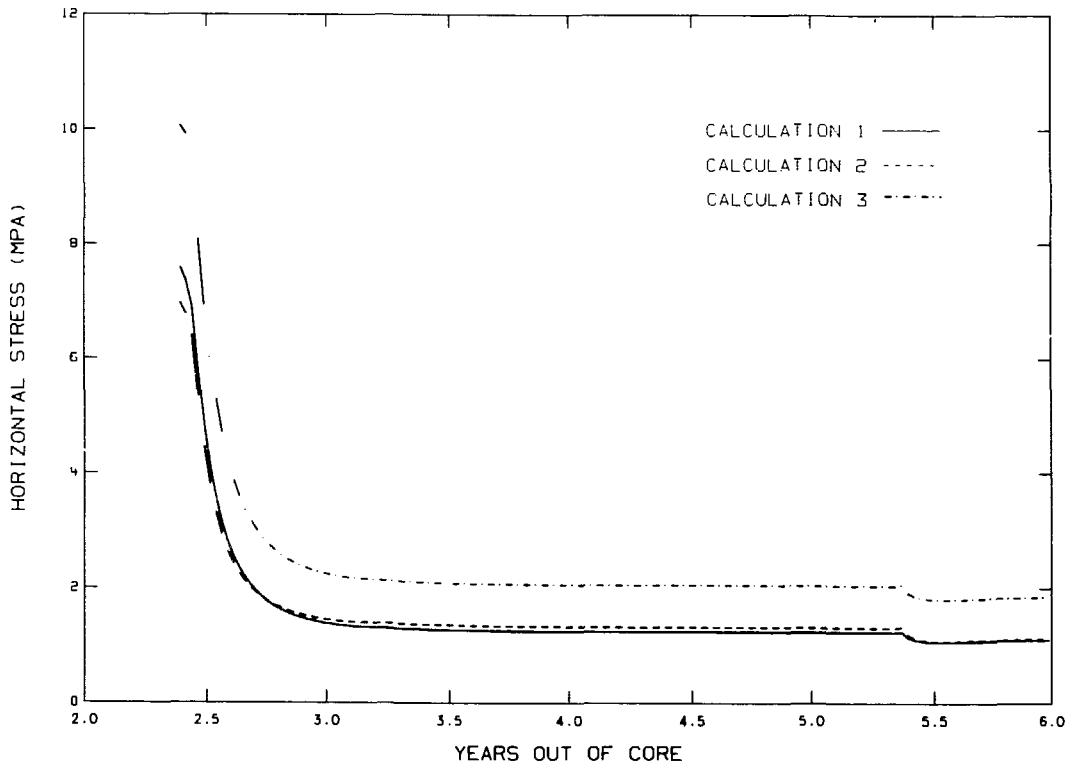

Figure 11a. Calculated in-plane horizontal stress vs time for a point at mid-height in pillar 3 m from heater drift.

spent fuel canister drift. Figures 13a and b show similar results from a point in the floor of the canister drift at midpoint elevation of the center spent-fuel canister, and 1.18 m radially outward from its centerline.

Comparing the results of these calculations, we see moderate differences between calculations 1 and 2 where the mesh loading is the same but the deformation moduli differ by about 40%. Larger differences occur in calculation 3 where the mesh loading is about 80% greater than in the other calculations.

The vibrating-wire stress gauges failed early in the test, making it impossible to compare calculations with data during most of the heating phase of the test. These failures occurred when

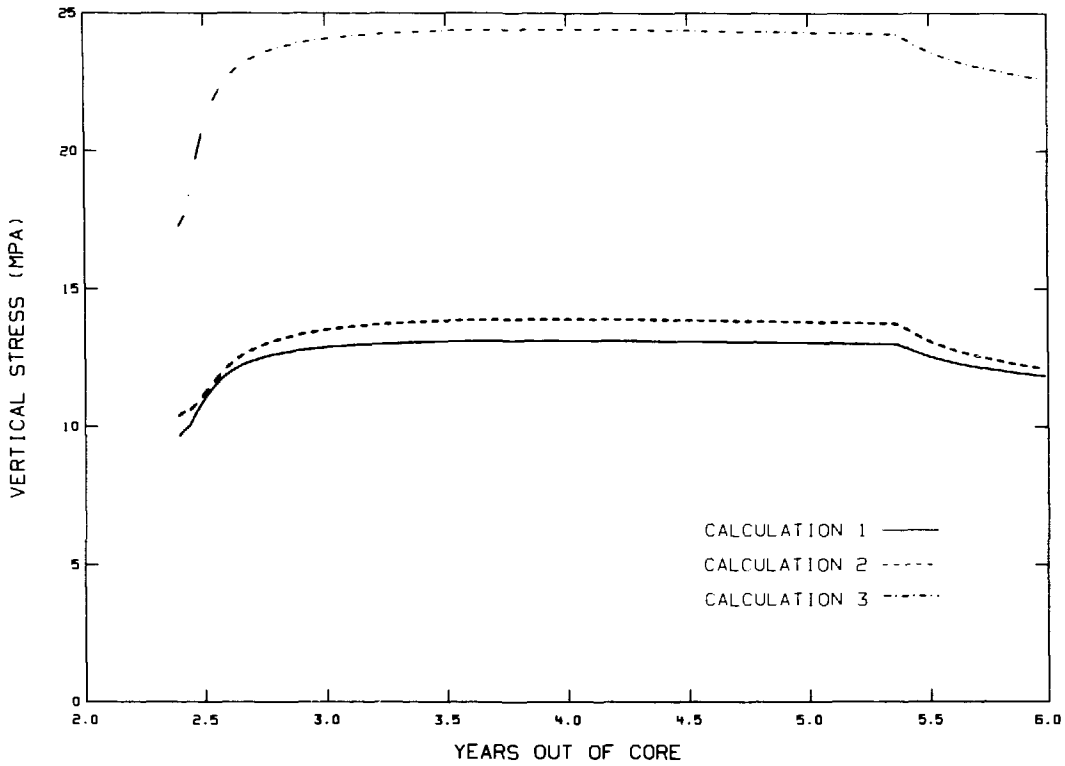

Figure 11b. Calculated in-plane vertical stress vs time for a point at mid-height in pillar 3 m from heater drift.

the gauge housings leaked, corroding the wire (Patrick et al., 1981). The instrument was redesigned with better seals and was re-installed at a time near the end of the heating cycle, shortly before the spent fuel was removed. Stress measurements at the three locations cited above were available from this time through the cooldown period.

To make these comparisons, we used the results from the stress-gauge rosettes to calculate secondary principal stresses for times of interest. From these, we determined the horizontal stress component in the plane of the calculation. Vertical in-plane stress values were measured directly using stressmeters in the horizontal boreholes, which are located mid-height in the ribs at two stations (Figs. 4a and b).

Table 6 shows comparisons of measured stress differences at the two stations for each gauge position and those calculated for the position between 5.35 and 5.85 YOC for each location. In comparing the measurements and calculations, the accuracy of the measurements must be considered. Patrick, Rector, and Scarafiotti (1984) report post-test calibrations for the stressmeters that show errors in the range of $\pm 50\%$ of the gauge readings. The measured and calculated changes in stress agree within the uncertainties of the measurements.

Tunnel Closure

Measurements of drift deformations were made routinely since the emplacement of the spent fuel. Both horizontal and vertical measurements were taken at five locations along the heater drifts and at six locations along the canister drift (Figs. 4a and b). Two types of instrumentation were used: convergence wire extensometers that were monitored automatically, and a manually operated tape extensometer with which measurements were made periodically, typically once each month. The tape extensometer measurements were initiated six weeks after the emplacement of the spent fuel.

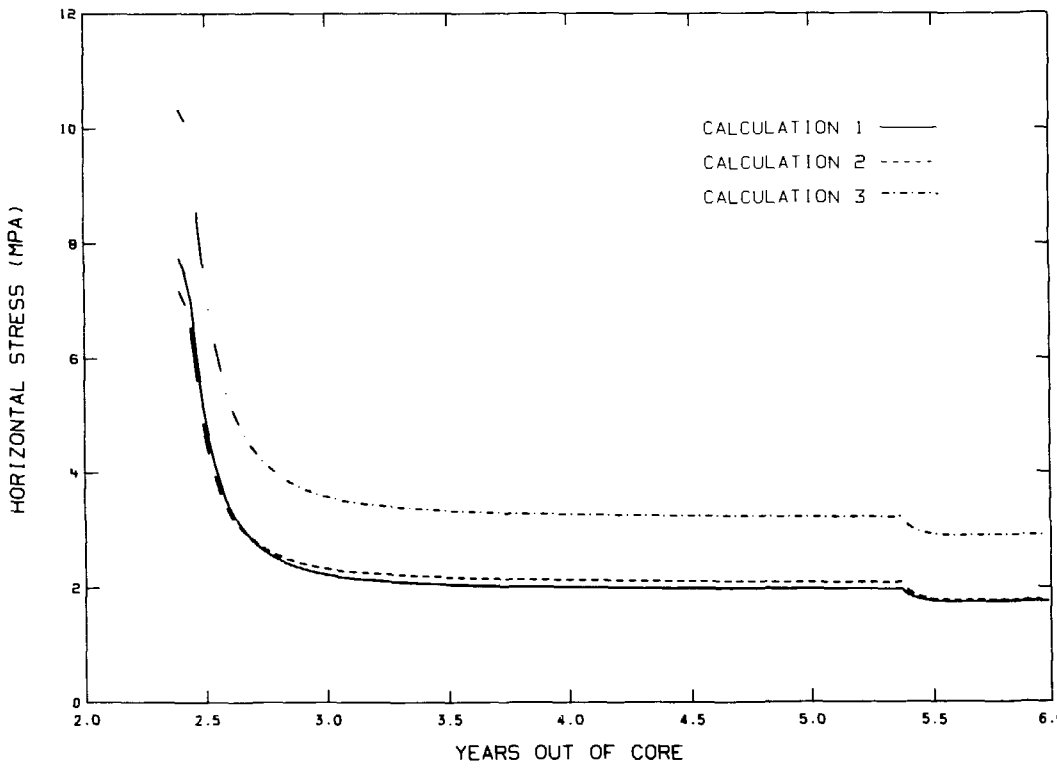

Figure 12a. Calculated in-plane horizontal stress vs time for a point mid-height in pillar 0.7 m from spent fuel drift.

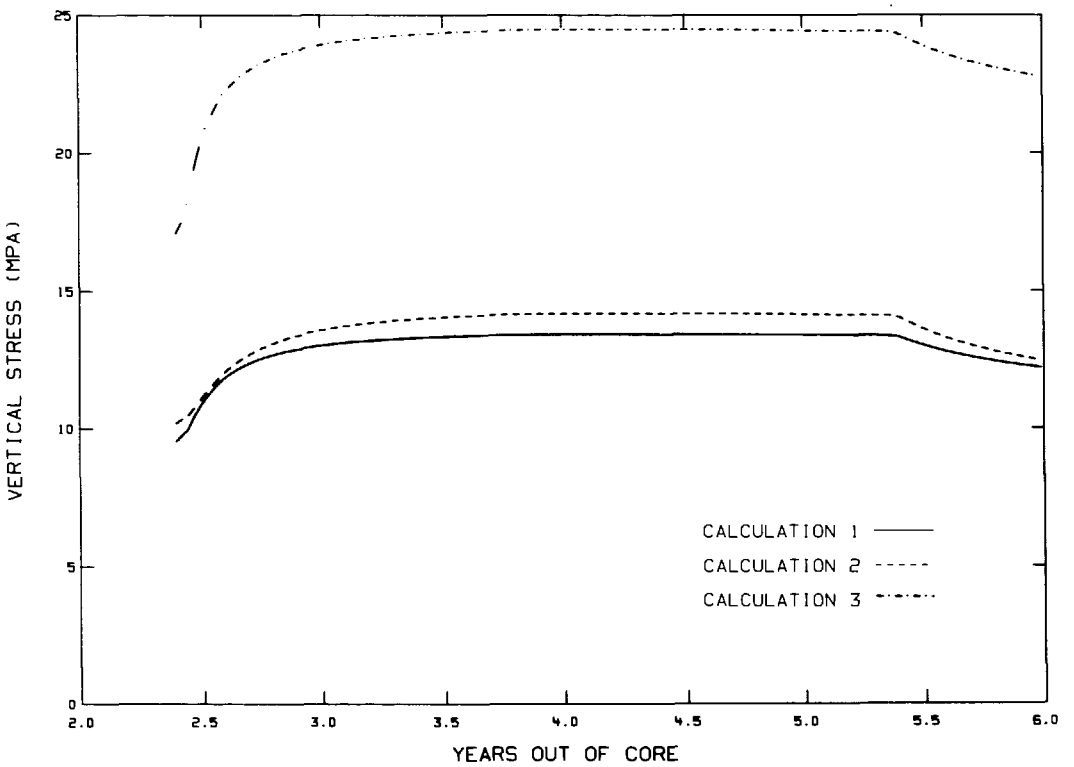

Figure 12b. Calculated in-plane vertical stress vs time for a point mid-height in pillar 0.7 m from spent fuel drift.

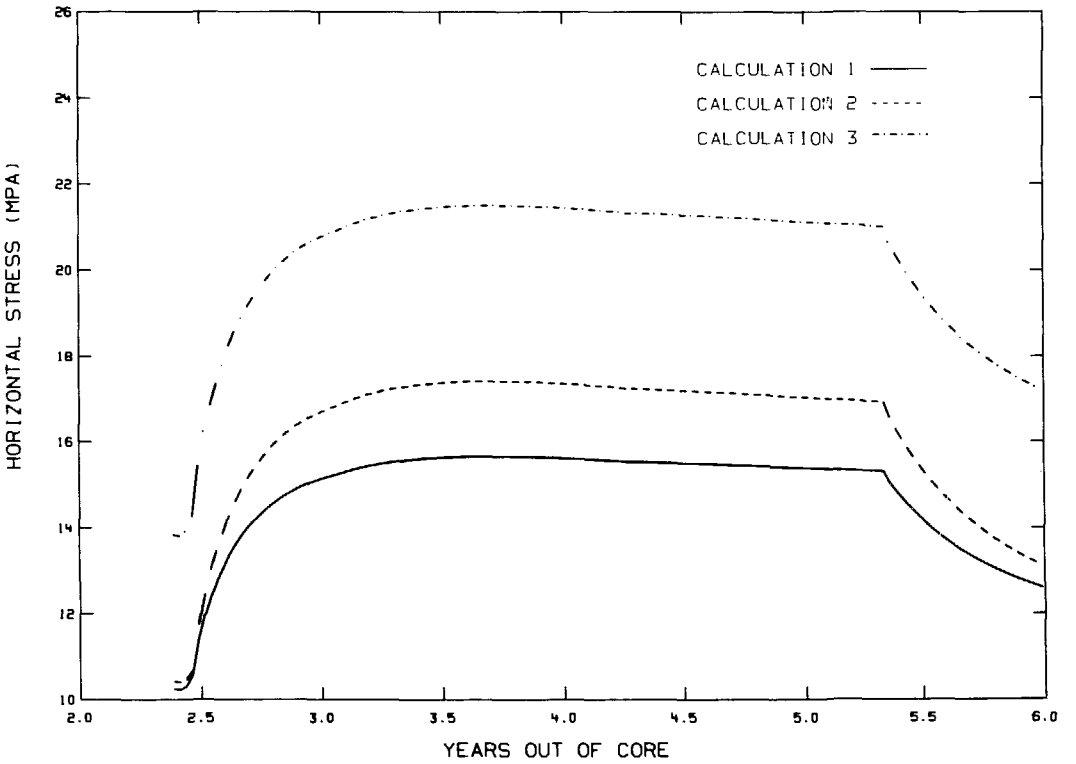

Figure 13a. Calculated in-plane horizontal stress vs time for a point at mid-point elevation of the spent-fuel canister, 1.8 m from its axis.

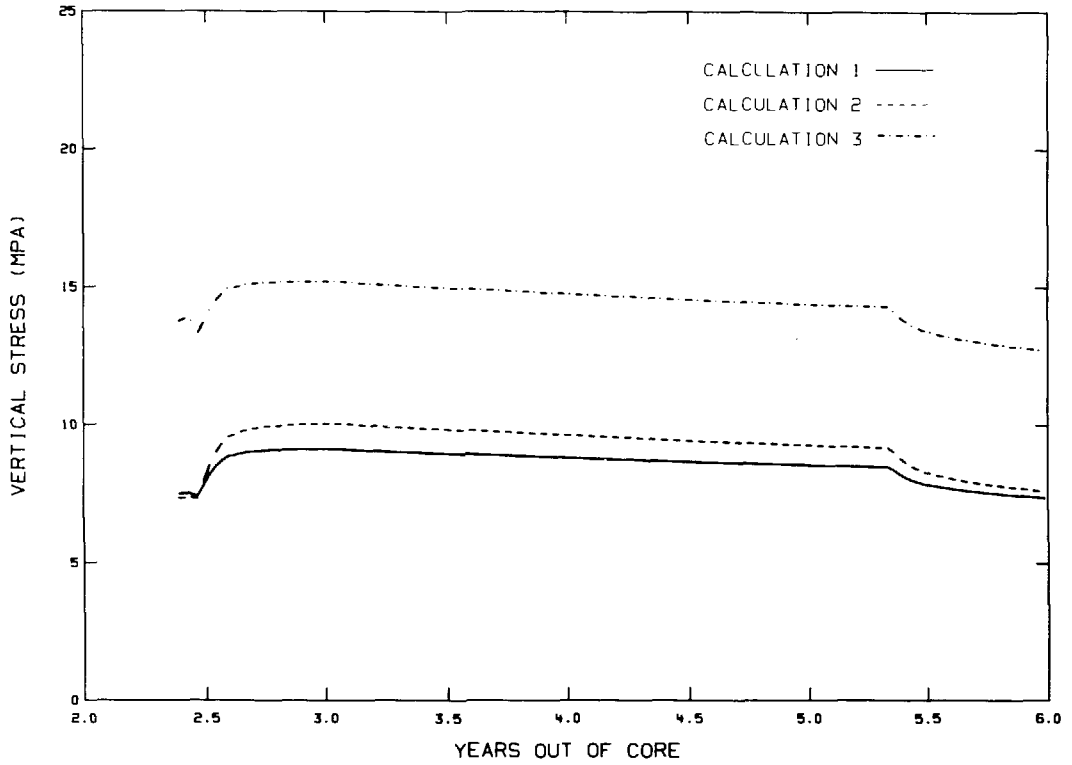

Figure 13b. Calculated in-plane vertical stress vs time for a point at mid-point elevation of spent-fuel canister, 1.18 m from its axis.

Table 6. Comparison of measured and calculated stress changes during cooldown period following removal of spent fuel.

Measured stress change (MPa)		Calculated stress changes (MPa)		
		#1	#2	#3
Horizontal in-plane stress 1.18 m from spent fuel at mid-point elevation				
Station 3 + 58	3.5	2.4	3.4	3.4
Station 2 + 98	3.3			
Vertical in-plane stress at mid-height in rib 0.7 m from canister drift				
Station 2 + 85	2.1	1.0	1.5	1.4
Station 3 + 47	0.9			
Vertical in-plane stress at mid-height in rib at mid-rib				
Station 2 + 28	0.6	1.1	1.4	1.4
Station 3 + 47	0.3			

Figures 14a and b show the horizontal and vertical spent fuel drift closures for each calculation, and Figs. 15a and b show the corresponding calculated closures for the heater drifts. The results of these calculations show the complexity of the effects of varying *in situ* stresses and moduli. At all locations, calculation 2 provides the smallest tunnel closures because it used both the lower *in situ* stress and higher moduli. Although calculation 1 shows the greatest horizontal convergence in the canister drift, there is essentially no difference between calculations 1 and 3 in the heater drift, even though the *in situ* stresses are markedly higher for calculation 3 (Table 5). Figures 14b and 15b show that calculation 3 does provide the greatest vertical tunnel closure in both the canister and heater drifts.

Measurements from five locations in the canister drift, five locations in the north heater drift, and four locations in the south heater drift can be compared with calculated displacements. Temperature-corrected tape extensometer measurements from redundant measurements and different operators were arithmetically averaged to produce single closure curves for the horizontal and vertical directions in each drift using techniques described by Yow and Butkovich (1982), Butkovich et al. (1982), and Patrick et al. (1981). Variations between locations, which range upward to plus or minus 0.2 mm, have not been correlated with specific variations in local properties and geologic structures, and hence are taken to be random in this analysis. Studies of the spacial variability in rock response are in progress.

The calculations show that as much as two-thirds of the maximum closure took place before the first tape extensometer measurements were made. As a result, it was necessary to add the amount of calculated closure to the averaged measured values to facilitate a comparison. For this, calculation 2 was chosen because it used average values of measured modulus and mesh loading based on best estimates of *in situ* stress (Table 5). Figures 16a and b show the comparison between horizontal and vertical canister drift closure, and Figs. 17a and b and 18a and b show similar comparisons for the north and south heater drifts, respectively.

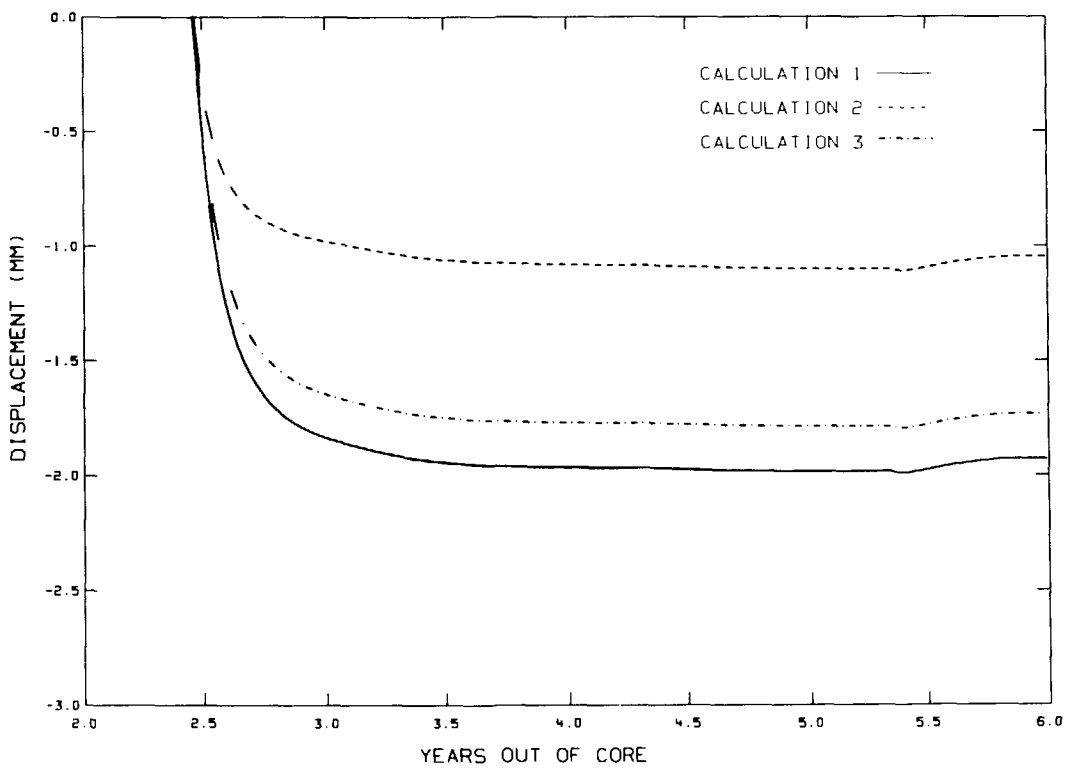

Figure 14a. Calculated horizontal closure of the spent fuel drift.

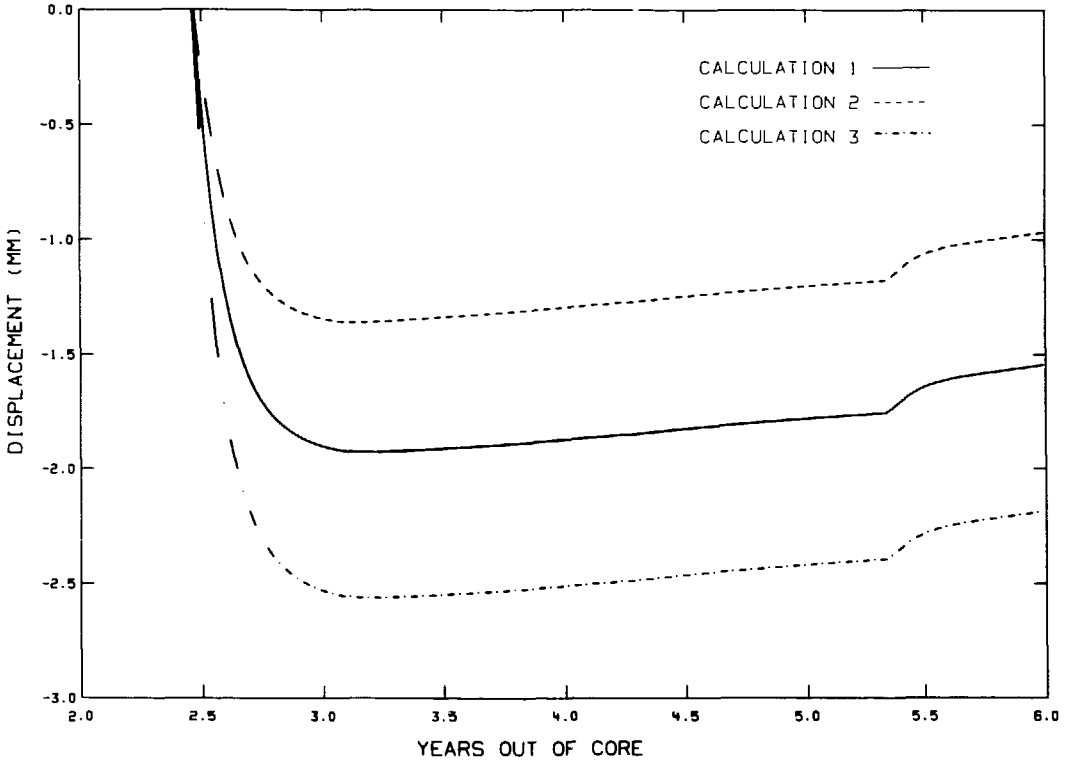

Figure 14b. Calculated vertical closure of the spent fuel drift.

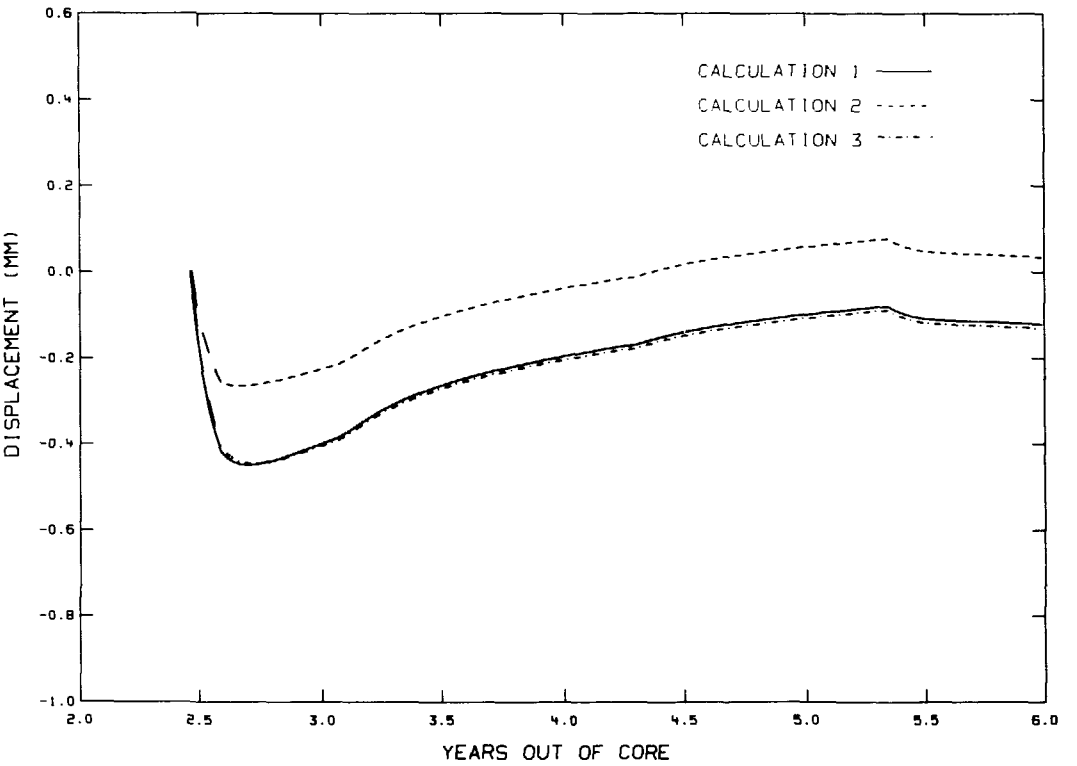

Figure 15a. Calculated horizontal closure of the heater drift.

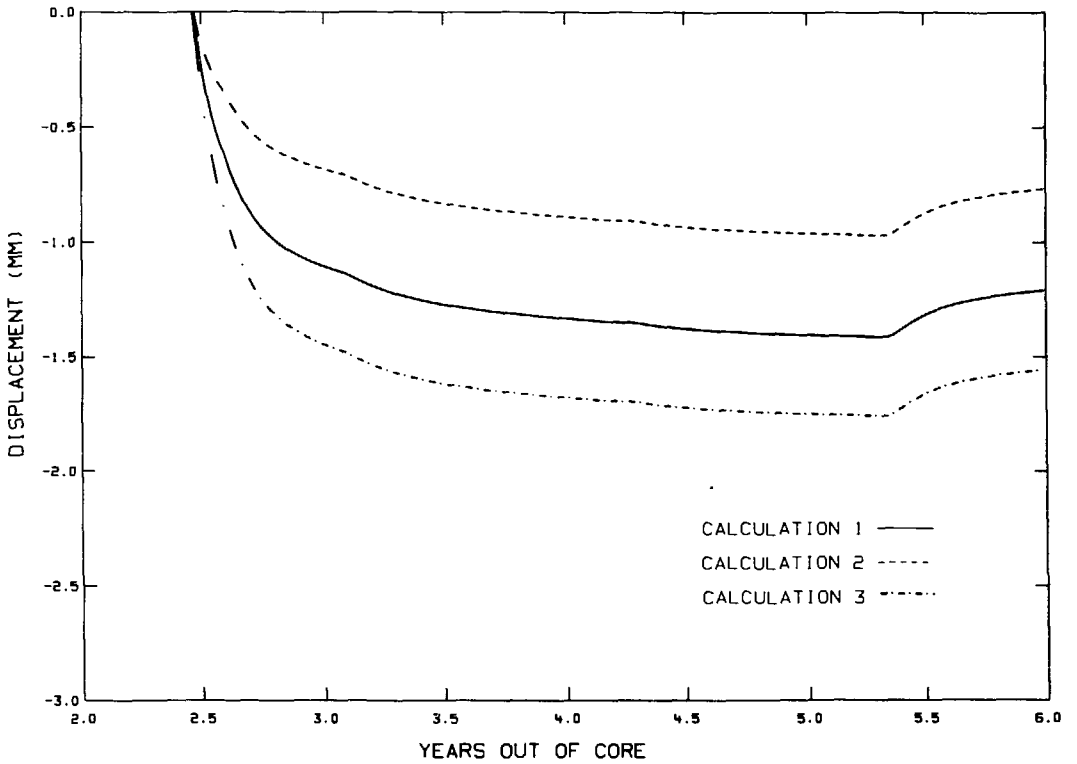

Figure 15b. Calculated vertical closure of the heater drift.

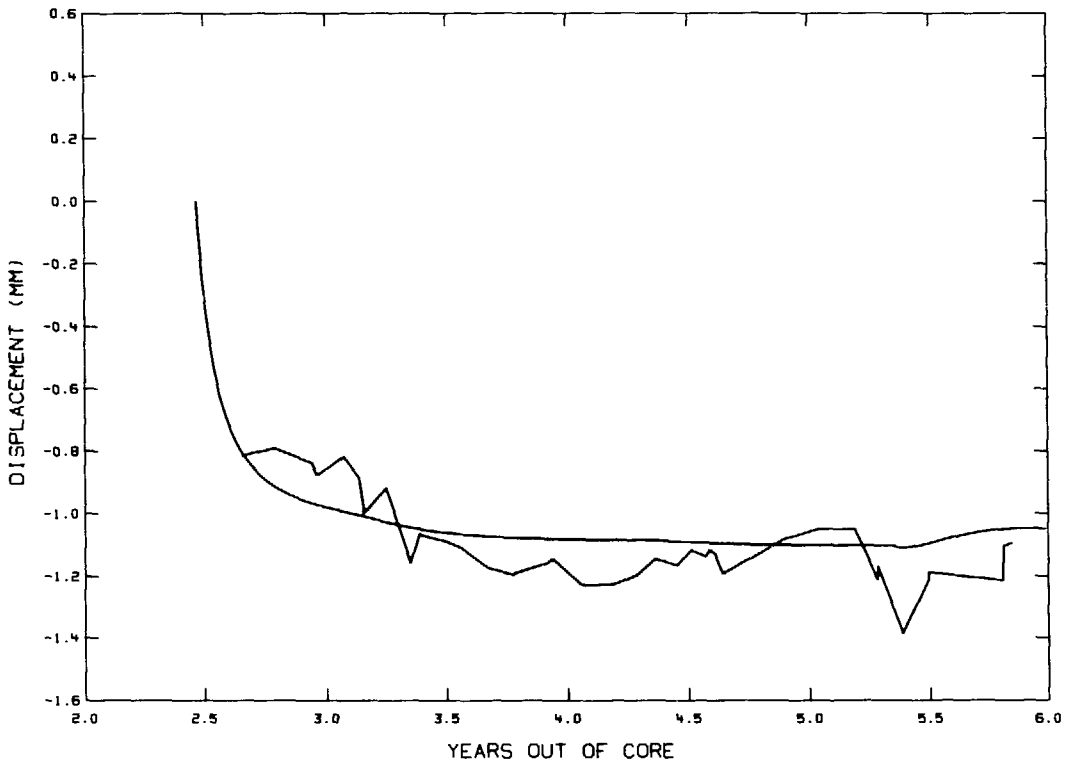

Figure 16a. Calculation 2 results compared with measured horizontal closure of the canister drift.

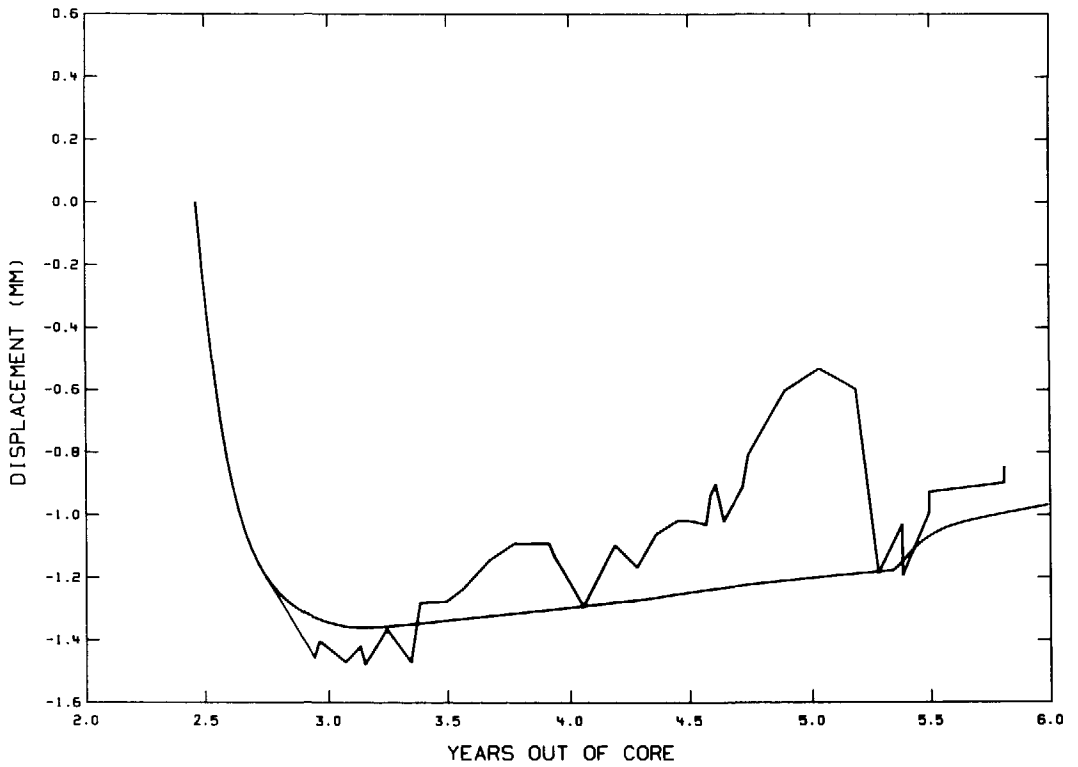

Figure 16b. Calculation 2 results compared with measured vertical closure of the canister drift.

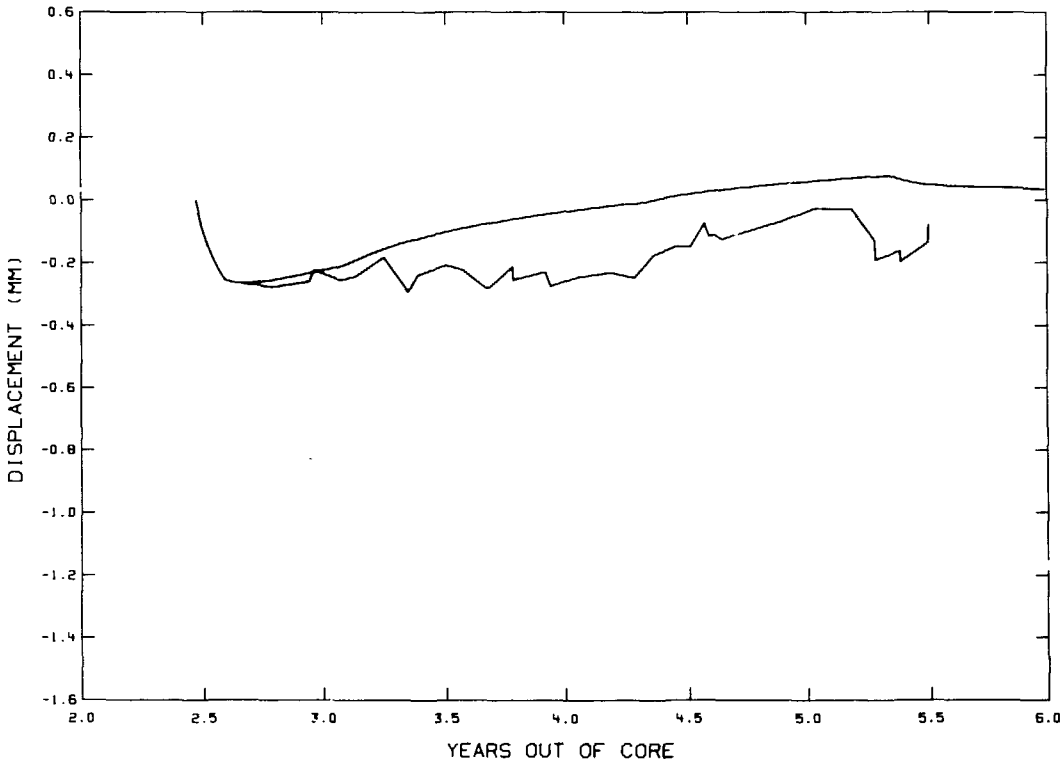

Figure 17a. Calculation 2 results compared with measured horizontal closure of the north heater drift.

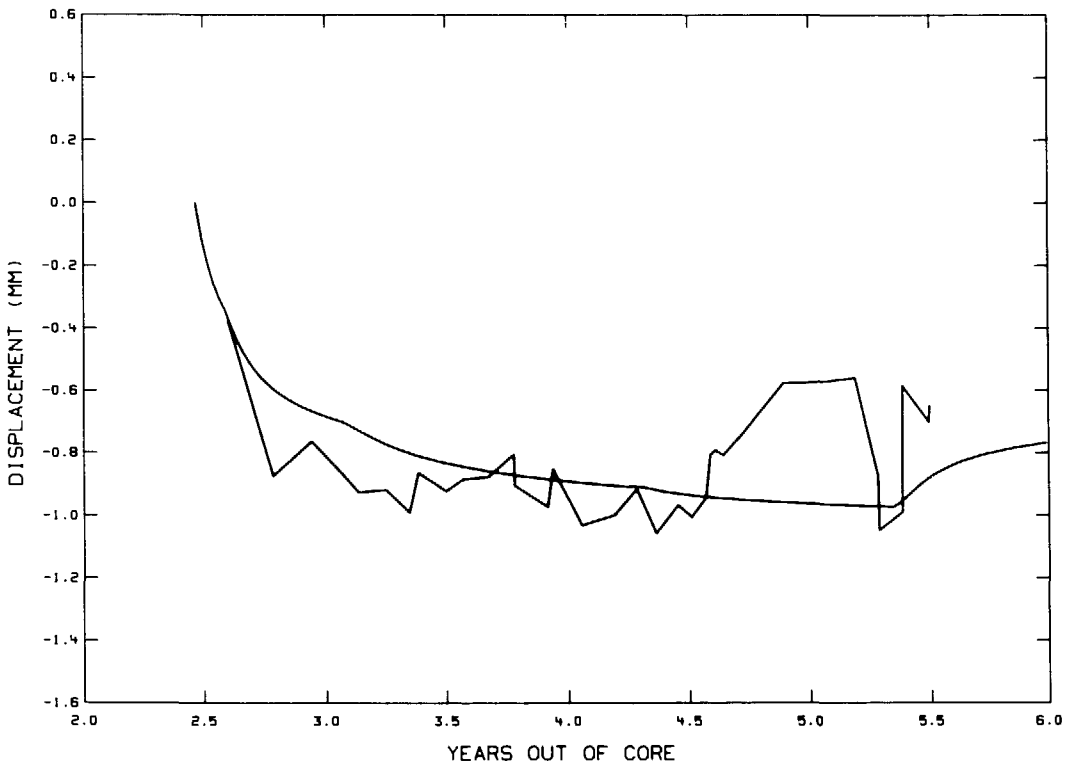

Figure 17b. Calculation 2 results compared with measured vertical closure of the north heater drift.

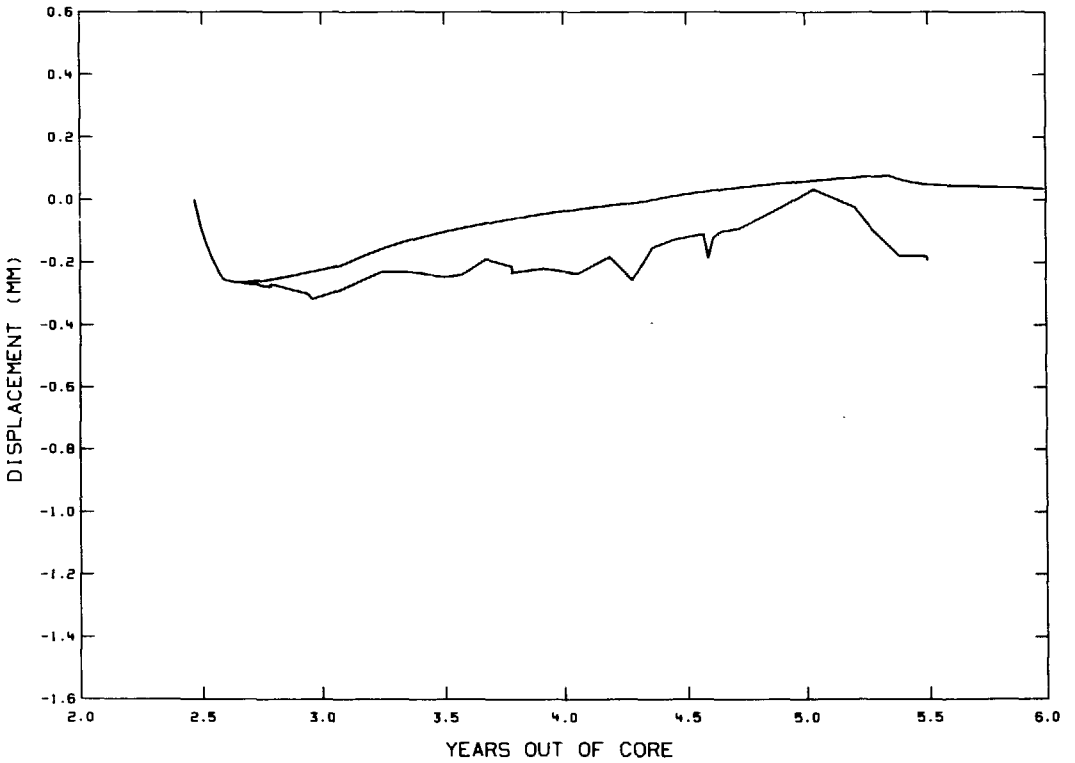

Figure 18a. Calculation 2 results compared with measured horizontal closure of the south heater drift.

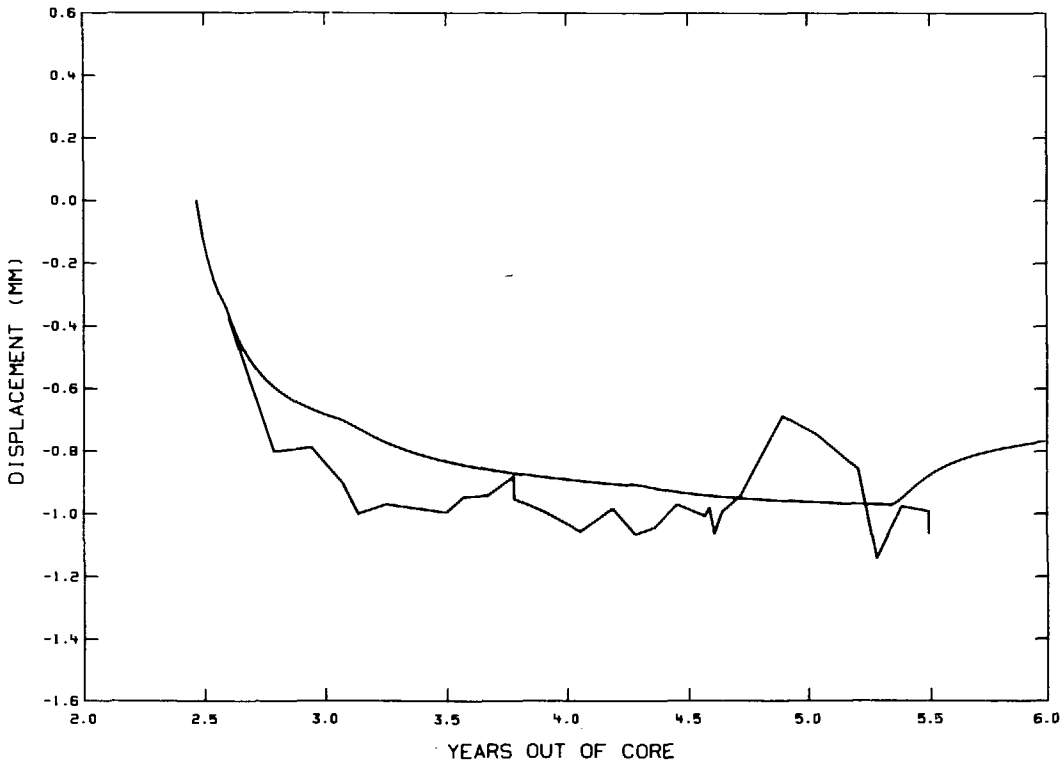

Figure 18b. Calculation 2 results compared with measured vertical closure of the south heater drift.

Although the averaged measurements appear somewhat erratic because of the marginally acceptable resolution of the instrument (about 0.025 mm), the calculations and measurements track each other quite well. First, one can see that the measured and calculated tunnel closures are similar in form. For the measurements showing closure during the entire heating period, the calculational results also show this effect. Where the measurements show closure followed by dilation, the calculation also shows this effect. Second, the magnitudes of closures provided by calculation 2 appear to be in good agreement with the measured responses. This may be seen by comparing Figs. 14a and 16a, 14b and 16b, 15b and 17b, and 15b and 18b. Only in the case of horizontal closure of the heater drifts (Figs. 15a, 17a, and 18a) does it appear that calculations 1 or 3 could have given somewhat better results.

When the difference between measurements and calculations is considered, note that the fractional difference should be based on the total closure. Measurements began toward the end of a period when the closure rates were quite high. Therefore, a small change from the assumption that both curves are connected at the time of the first measurement can dramatically change the agreement between measurement and calculation.

At the time of the writing of this report, the convergence wire extensometer data obtained through the central data acquisition system were unavailable for analysis and inclusion here.

Relative Displacements of the Rock Mass

Temperature-corrected measurements within the rock mass can also be compared with calculations. The finite-element mesh nodal points that were selected for these comparisons were near or intersected by the positions of the horizontal and inclined borehole rod extensometers (Figs. 4a and b). Since the calculations provide horizontal and

vertical displacement components, it was necessary to trigonometrically project these components onto the 34° and 50° inclined positions that correspond to the extensometers. We then interpolated between nearby nodal points to obtain a calculated vector displacement to compare with the appropriate measured displacement.

Corrections were made for the thermal expansion of the rods. These corrections were, in every case, a factor of two or more larger than the recorded displacements. This is because the coefficients of expansion of the steel rods from which the rod extensometers were made are similar to those of the rock. That is, both the rock and instruments expand nearly the same amount under a given temperature change. As a result, the measured displacements contain a large component from the expansion of the instrument, a small component reflecting the difference between rock and instrument expansion, and a possible third component due to inelastic rock response.

Once again, no data were available for the early part of the test so it was necessary to make all comparisons relative to a spent-fuel age of 3.0 YOC, approximately 6 months after emplacement of the spent fuel. The comparisons between measurements and calculations for each anchor point location and for each of the three calculations are presented in Appendix A for four different times: 3.5, 4.5, 5.25, and 5.85 YOC (1 and 2 years after start of test, at the end of the heating cycle, and at the end of the 6-month cooldown period).

The data provided in Appendix A are summarized for ease of analysis in Figs. 19a–c. Here we plot the 230 measured and calculated displacements against each other, fit a line through the points, and provide some basic measures of how well the data compare with the calculations. Calculation 2 is nominally better than the other calculations by all three measures. While the R^2 is rather low (RR = 0.574), it is somewhat better than the 0.517 and 0.526 of calculations 1 and 3,

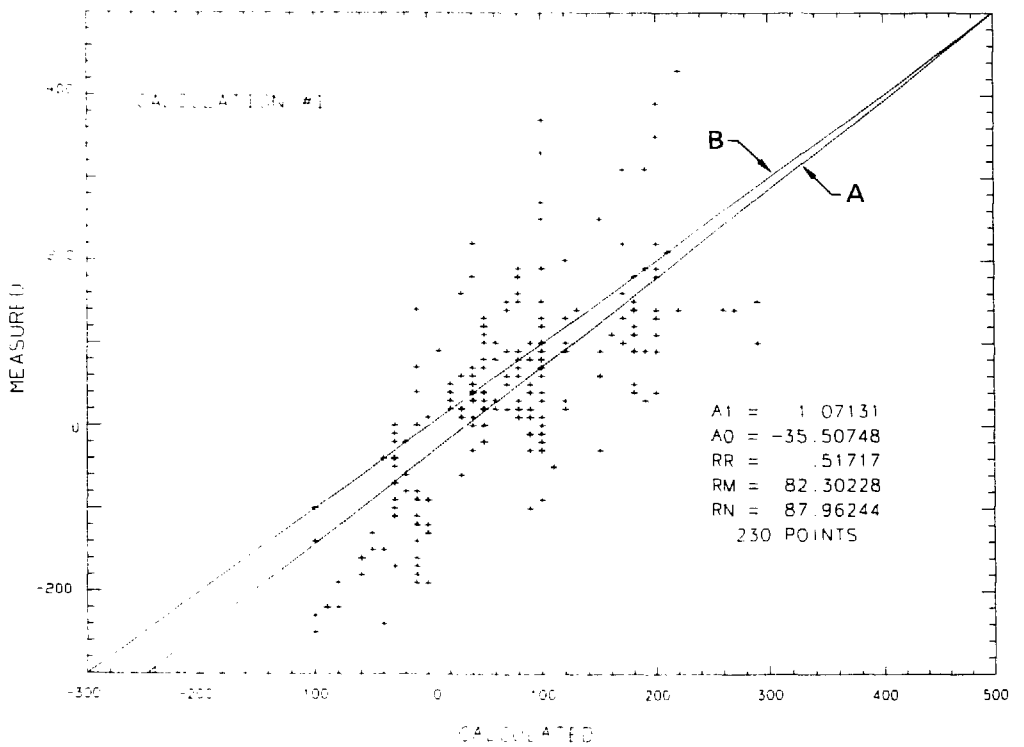

Figure 19a. Comparison of measured displacements with the results of calculation 1 (units in μm). Coefficients A1 and A0 give the slope and y-intercepts, respectively, for best fit line A. Line B has values of 1.0 and 0.0.

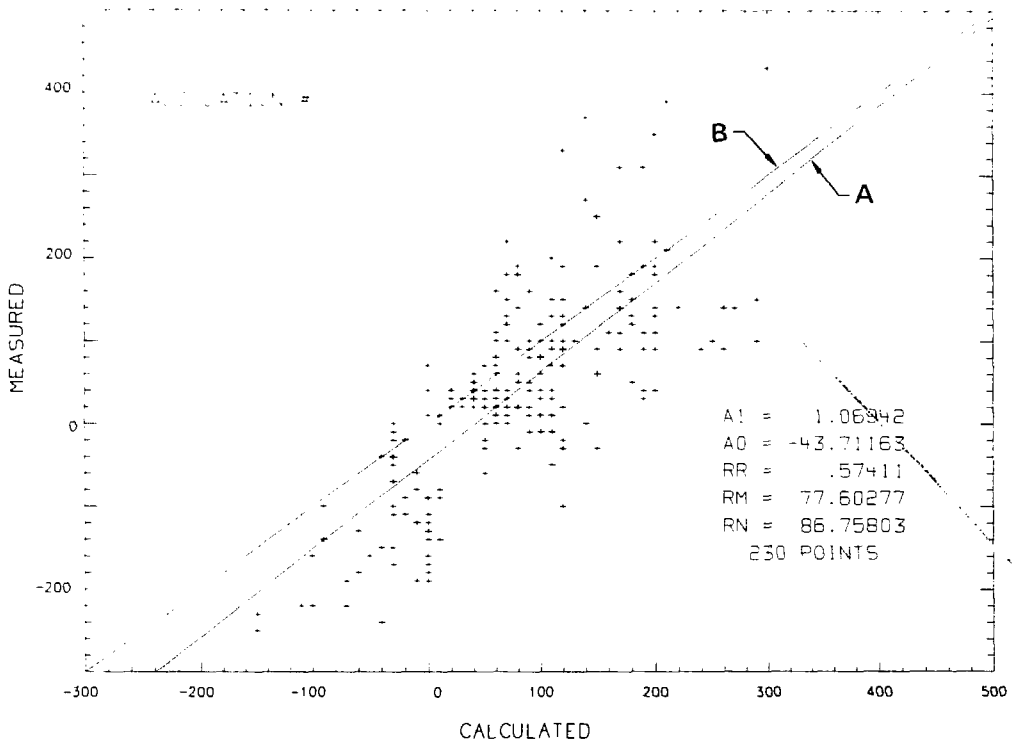

Figure 19b. Comparison of measured displacements with the results of calculation 2 (units in μm). Coefficients A1 and A0 give the slope and y-intercepts, respectively, for best fit line A. Line B has values of 1.0 and 0.0.

respectively. In addition, the root-mean-square error of the data with respect to the least-squares fit is about 5 μm less for calculation 2. The relatively small R^2 and large RMS error can be explained, in large part, by errors in the instrumentation. *In situ* calibrations indicated errors of about 10 $\pm$ 60 μm (at one σ) with errors for individual instruments ranging $\pm$0.25 mm (Patrick, Rector, and Scarafiotti, 1984). Therefore, the data and calculations cannot agree any better than this.

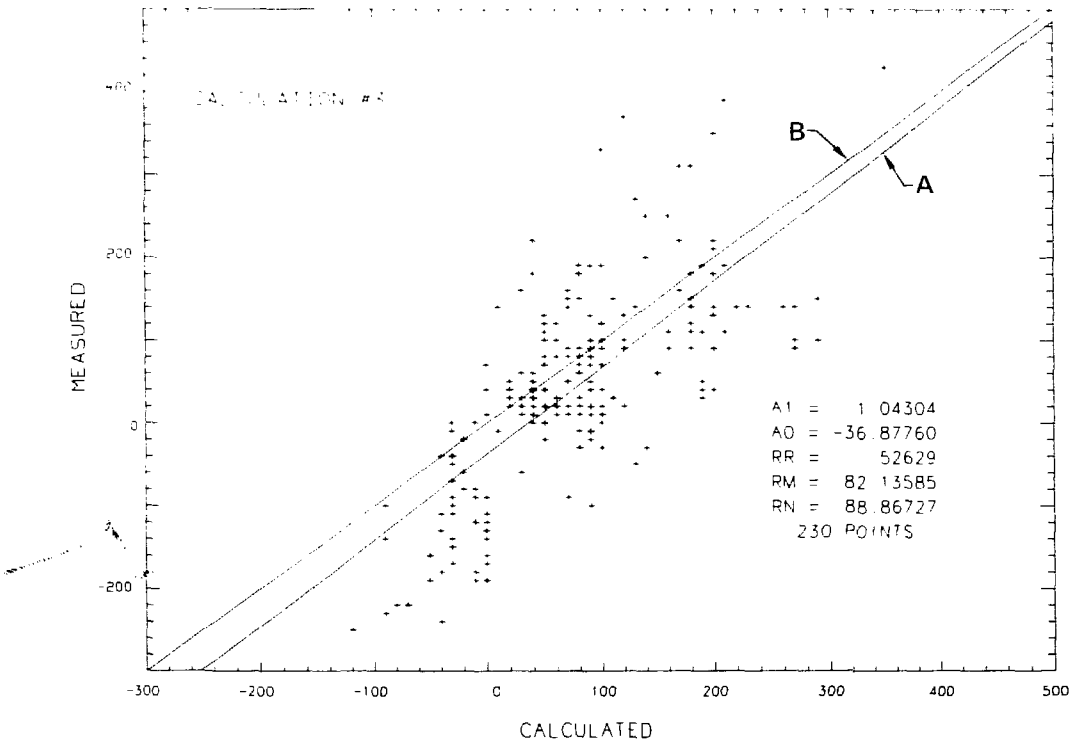

Figure 19c. Comparison of measured displacements with the results of calculation 3 (units in μm). Coefficients A1 and A0 give the slope and y-intercepts, respectively, for best fit line A. Line B has values of 1.0 and 0.0.

Conclusions

The SFT—C caused extensive heating of a large volume of granitic rock. Although other tests of this type have been conducted, this was the first opportunity to evaluate the ability of a finite-element code such as ADINA to calculate thermomechanical responses of rock on this large a scale. Calculations were performed using the best available thermomechanical properties and *in situ* stresses for the rock surrounding the mined openings that comprised the SFT—C. The ADINA calculations all used an isotropic thermoelastic model with temperature-dependent thermal expansion coefficients.

In general, the measured and calculated displacements agreed within the accuracy of the instrumentation. In spite of the fractured condition of the rock mass identified during structural geology mapping (Wilder and Yow, 1984), the rock mass appeared to have behaved essentially thermoelastically. This conclusion is tempered by the fact that measurements were not obtained at early times when rates of displacements and stress changes were very high and when up to two-thirds of the total calculated responses occurred. Furthermore, intrinsic limitations of transducer accuracies make highly precise comparisons between data and calculations impossible.

Within these limitations, we conclude that calculation 2 provided the best agreement with the data. This calculation used average rock-mass moduli, a 0.5-m-thick explosively damaged zone around each opening, and the average *in situ* stress magnitudes that resulted in a horizontal-to-vertical stress ratio of 1.2.

Acknowledgments

Overall guidance for this and other NNWSI projects at LLNL is provided by L. Ramspott. We thank L. Ballou, F. Heuze, and J. Yow, Jr., for their careful reviews and constructive comments on this report. D. N. Montan provided support in the statistical analysis of the comparisons between measurements and calculations.

Special appreciation is extended to L. Grabowski, who typed the original manuscript, P. Proctor, who drafted some of the figures, and M. Donohue, who provided editorial services.

Bibliography

Bathe, K. J. (1977), *ADINAT, A Finite Element Program for Automatic Dynamic Incremental Analysis of Temperature*, Massachusetts Institute of Technology, Cambridge, MA, Rept. No. 82448-5.

Bathe, K. J. (1978), *ADINA, A Finite Element Program for Automatic Dynamic Incremental Nonlinear Analysis*, Massachusetts Institute of Technology, Cambridge, MA, Rept. No. 82448-1.

Brough, W. G., and W. C. Patrick (1982), *Instrumentation Report #1, Specifications, Design, Calibration, and Installation of Instrumentation for an Experimental, High Level, Nuclear Waste Storage Facility*, Lawrence Livermore National Laboratory, Livermore, CA, UCRL-53248.

Butkovich, T. R. (1980), *Mechanical and Thermomechanical Calculations Related to the Storage of Spent Nuclear Fuel Assemblies in Granite*, Lawrence Livermore National Laboratory, Livermore, CA, UCRL-52985.

Butkovich, T. R., and D. N. Montan (1980), *A Method for Calculating Internal Radiation and Ventilation with the ADINAT Heat-Flow Code*, Lawrence Livermore National Laboratory, Livermore, CA. UCRL-52918.

Butkovich, T. R. (1981), *As-Built Mechanical and Thermomechanical Calculations of a Spent-Fuel Test in Climax Stock Granite*, Lawrence Livermore National Laboratory, Livermore, CA, UCRL-53198.

Butkovich, T. R., J. L. Yow, Jr., and D. N. Montan (1982), *Influence of Heat Flow on Drift Closure During Climax Granite Spent Fuel Test: Measurements and Calculations*, Lawrence Livermore National Laboratory, Livermore, CA, UCRL-87248.

Creveling, J. B., F. S. Shuri, K. M. Foster, and S. V. Mills (1984), *In Situ Stress Measurements at the Spent Fuel Test—Climax Facility*, Lawrence Livermore National Laboratory, Livermore, CA, Contractor Report UCRL-15628, Submitted by Foundations Sciences Inc., Portland, OR.

Edwards, A. L. (1972), *A Computer Program for Transient and Steady State Temperature Distribution in Multidimensional Systems*, Lawrence Livermore National Laboratory, Livermore, CA, UCRL-14754, Rev. 3.

Ellis, W. L. and J. Magner (1982), *Determination of the In Situ State of Stress at the Spent Fuel Test Site, Climax Stock, Nevada Test Site*, U.S. Geological Survey, Reston, VA, Open File Report 82-458.

Heard, H. C. (1980), "Thermal Expansion and Inferred Permeability of Climax Quartz Monzonite to 300 K and 27.6 MPa," *Int. J. Rock Mech. Min. Sci. and Geomech. Abst.* **17**, pp. 289–296.

Heuze, F., W. C. Patrick, R. V. de la Cruz, and C. F. Voss (1981), *In Situ Geomechanics Climax Granite, NTS*, Lawrence Livermore National Laboratory, Livermore, CA, UCRL-53076.

Heuze, F., T. R. Butkovich, and J. Peterson (1981), *An Analysis of the "Mine-By" Experiment in Climax Granite, Nevada Test Site*, Lawrence Livermore National Laboratory, Livermore, CA, UCRL-53133.

Montan, D. M., and W. E. Bradkin (1984), *Heater Test 1, Climax Stock Granite, Nevada*, Lawrence Livermore National Laboratory, Livermore, CA, UCRL-53496.

Montan, D. N., and W. C. Patrick (1981), *Thermal Calculations for the Design, Construction, Operation, and Evaluation of the Spent Fuel Test—Climax, Nevada Test Site*, Lawrence Livermore National Laboratory, Livermore, CA, UCRL-53238.

Patrick W. C., R. C. Carlson, and N. L. Rector (1981), *Instrumentation Report #2: Identification, Evaluation, and Remedial Actions Related to Transducer Failure at the Spent Fuel Test—Climax*, Lawrence Livermore National Laboratory, Livermore, CA, UCRL-53251.

Patrick, W. C., N. L. Rector, and J. J. Scarafiotti (1984), *Instrumentation Report #3: Performance and Reliability of Instrumentation Deployed for the Spent Fuel Test—Climax*, Lawrence Livermore National Laboratory, Livermore, CA, UCRL-53657.

Patrick, W. C., J. L. Yow, Jr., and M. C. Axelrod (1985), *Measurement of In Situ Deformability with the NX Borehole Jack, SFT—C, Nevada Test Site*, Lawrence Livermore National Laboratory, Livermore, CA, UCRL in preparation.

Patrick, W. C., T. R. Butkovich, R. C. Carlson, W. B. Durham, H. C. Ganow, G. L. Hage, E. L. Majer, D. N. Montan, R. A. Nyholm, N. L. Rector, F. J. Ryerson, H. Weiss, and J. L. Yow, Jr. (1982), *Spent Fuel Test—Climax: Technical Measurements Interim Report, Fiscal Year 83*, Lawrence Livermore National Laboratory, Livermore, CA, UCRL-53294-83.

Pratt, H., R. Lingle, and T. Schrauf (1979), *Laboratory Measured Material Properties of Quartz Monzonite, Climate Stock, Nevada Test Site*, Lawrence Livermore National Laboratory, Livermore, CA, UCRL-15073.

Ramspott, L. D., L. B. Ballou, R. C. Carlson, D. N. Montan, T. R. Butkovich, J. E. Duncan, W. C. Patrick, D. G. Wilder, W. G. Brough, and M. C. Mayr (1979), *Technical Concept for a Test of Geological Storage of Spent Reactor Fuel in the Climax Stock Granite, Nevada Test Site*, Lawrence Livermore National Laboratory, Livermore, CA, UCRL-52796.

Schmittroth, F., G. J. Neely, and J. C. Krogness (1980), *A Comparison of Measured and Calculated Decay Heat for Spent Fuel Near 2.5 Years Cooling Time*, Hanford Engineering Development Laboratory, Richland, WA, HEDL-TC-1759.

Schrauf, T. and M. Board (1979), *Instrument Selection, Installation, and Analysis of Data for the Spent Fuel Mine-By, Nevada Test Site, Climax Stock*, Lawrence Livermore National Laboratory, Livermore, CA, Contractor Report UCRL-15076.

Yow, J. L., Jr., and T. R. Butkovich (1982), *Calculated and Measured Drift Closure During the Spent Fuel Test in Climax Granite*, Lawrence Livermore National Laboratory, Livermore, CA, UCRL-87179.

Wilder, D. G., and J. L. Yow, Jr. (1984) *Structural Geology Report, Spent Fuel Test—Climax, Nevada Test Site*, Lawrence Livermore National Laboratory Livermore, CA, UCRL-53381.

MLD/lg

Appendix A

Appendix A gives plots of relative displacement measurements compared with calculational results for the three calculations discussed in the text. These measurements were made at two stations, designated as 2 + 83 and 3 + 45. The geological structure at one station is somewhat different from the other, as documented by Wilder and Yow (1984). Station 2 + 83 has five major shear joints passing through the ribs and intersecting the drifts, while Station 3 + 45 has two high-angle shear joints passing through the rib between the north heater drift and spent fuel drift.

The figures show the relative positions of anchor points at each station. The upper value is a measurement, and the lower value is obtained from calculated nodal point displacements that lie on or near the borehole positions in which the instruments are located. The results are interpolated to correspond with the position of the measurement. All values shown are given in millimeters of displacement since 3.0 YOC (about 0.5 year after start of heating), the time at which measurements from these instruments became available. A negative value indicates a shortening of the distance between the anchor point and the hole collar.

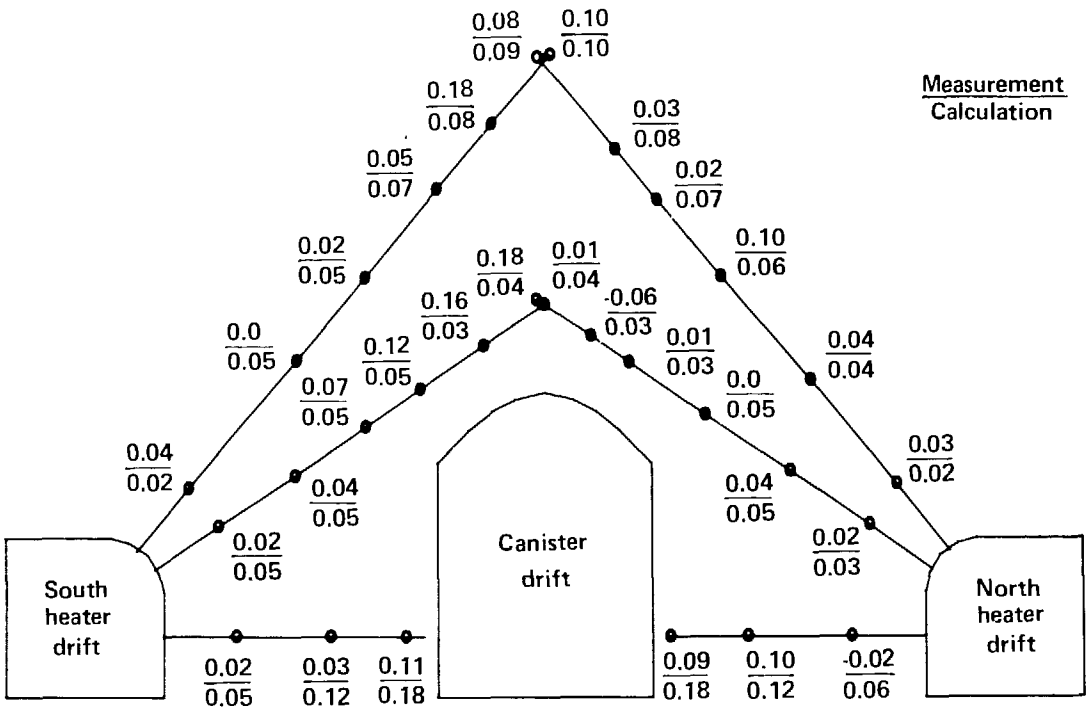

Figure A-1. Results from calculation 1 for Station 2 + 83 at 3.5 YOC.

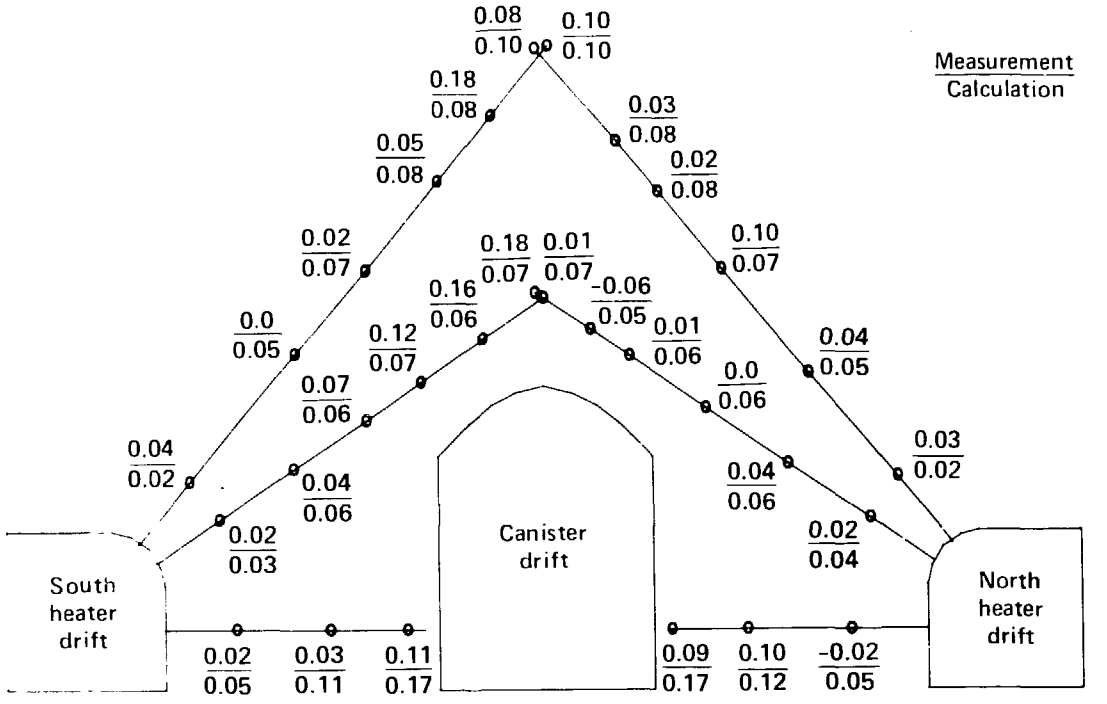

Figure A-2. Results from calculation 2 for Station 2 + 83 at 3.5 YOC.

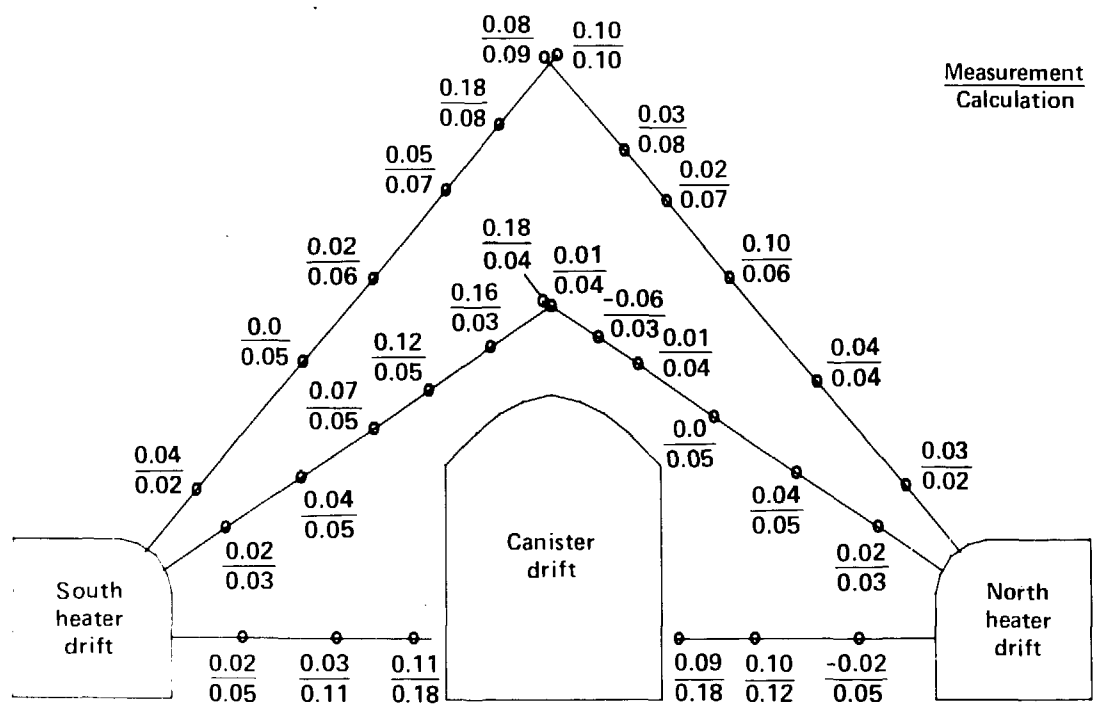

Figure A-3. Results from calculation 3 for Station 2 + 83 at 3.5 YOC.

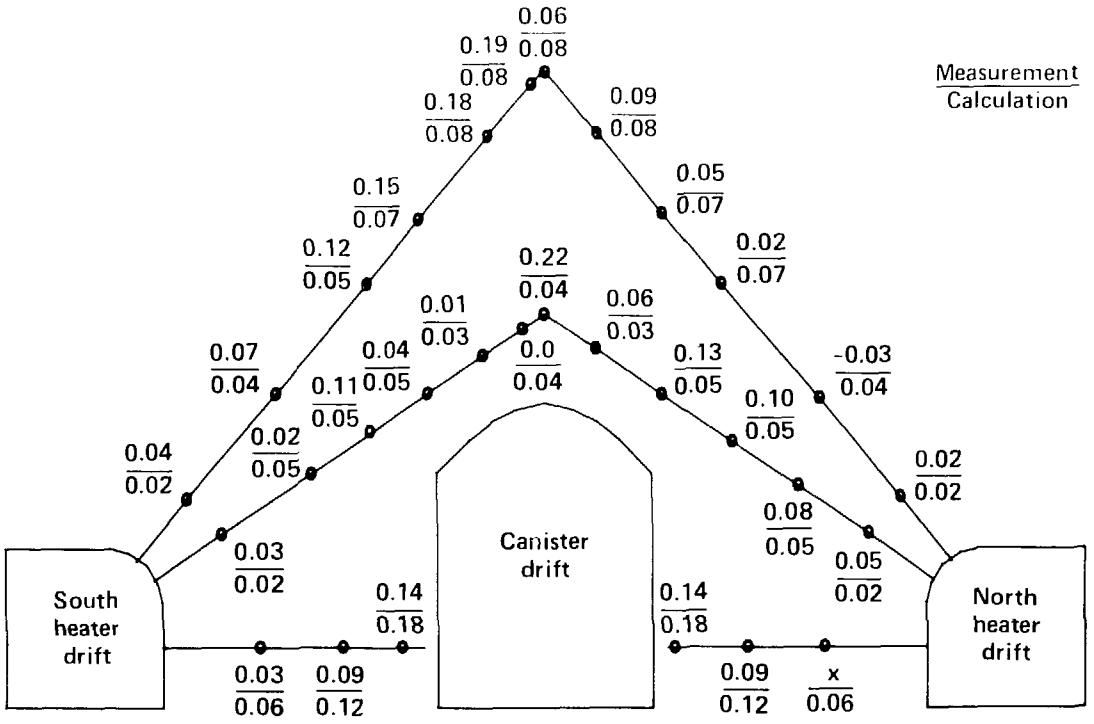

Figure A-4. Results from calculation 1 for Station 3 + 45 at 3.5 YOC.

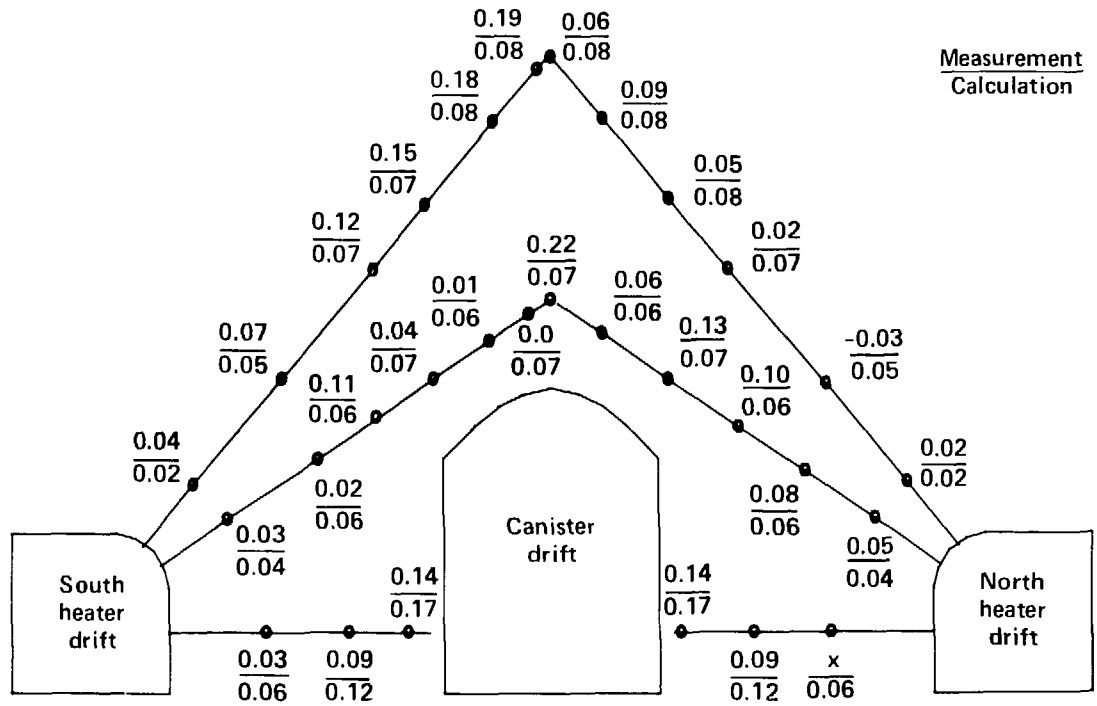

Figure A-5. Results from calculation 2 for Station 3 + 45 at 3.5 YOC.

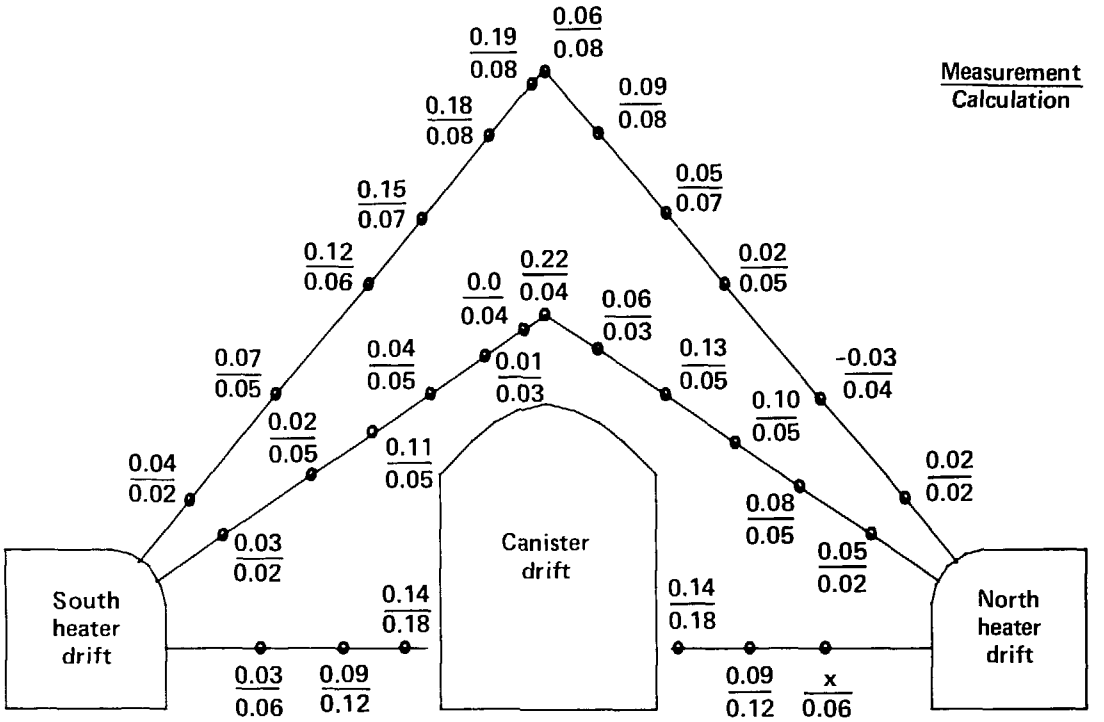

Figure A-6. Results from calculation 3 for Station 3 + 45 at 3.5 YOC.

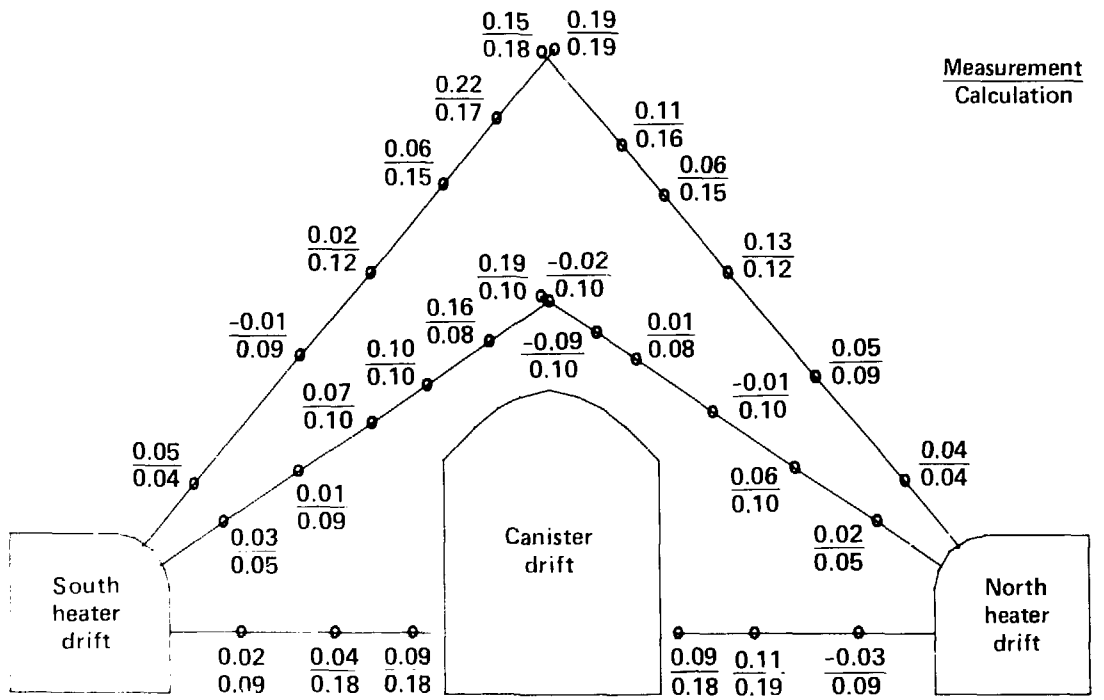

Figure A-7. Results from calculation 1 for Station 2 + 83 at 4.5 YOC.

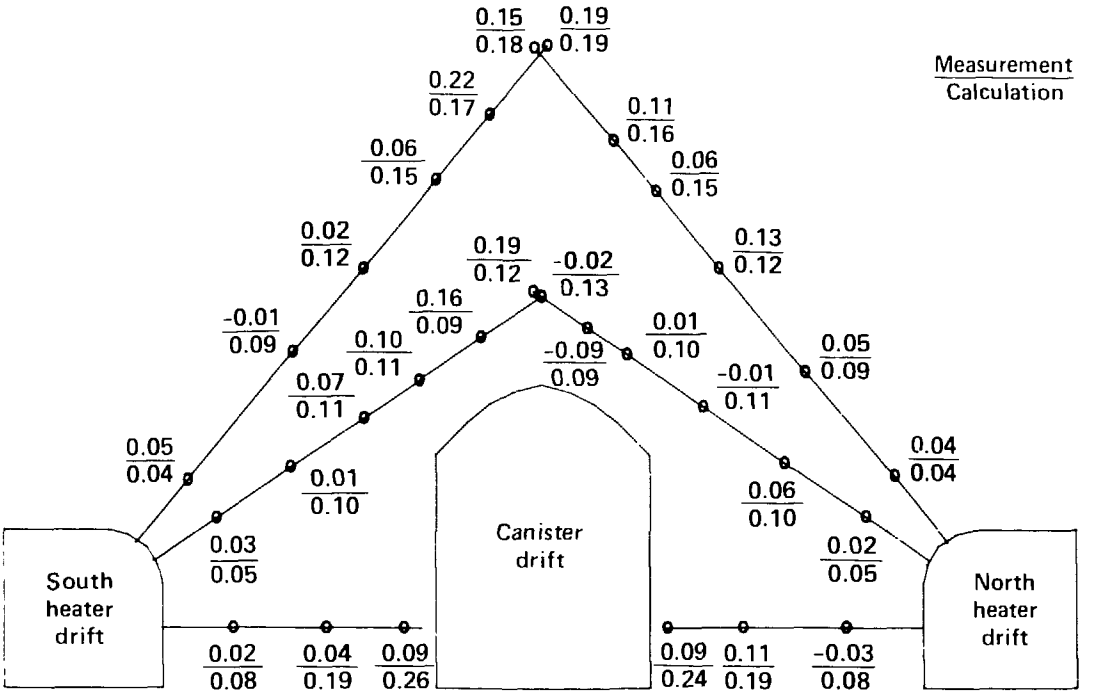

Figure A-8. Results from calculation 2 for Station 2 + 83 at 4.5 YOC.

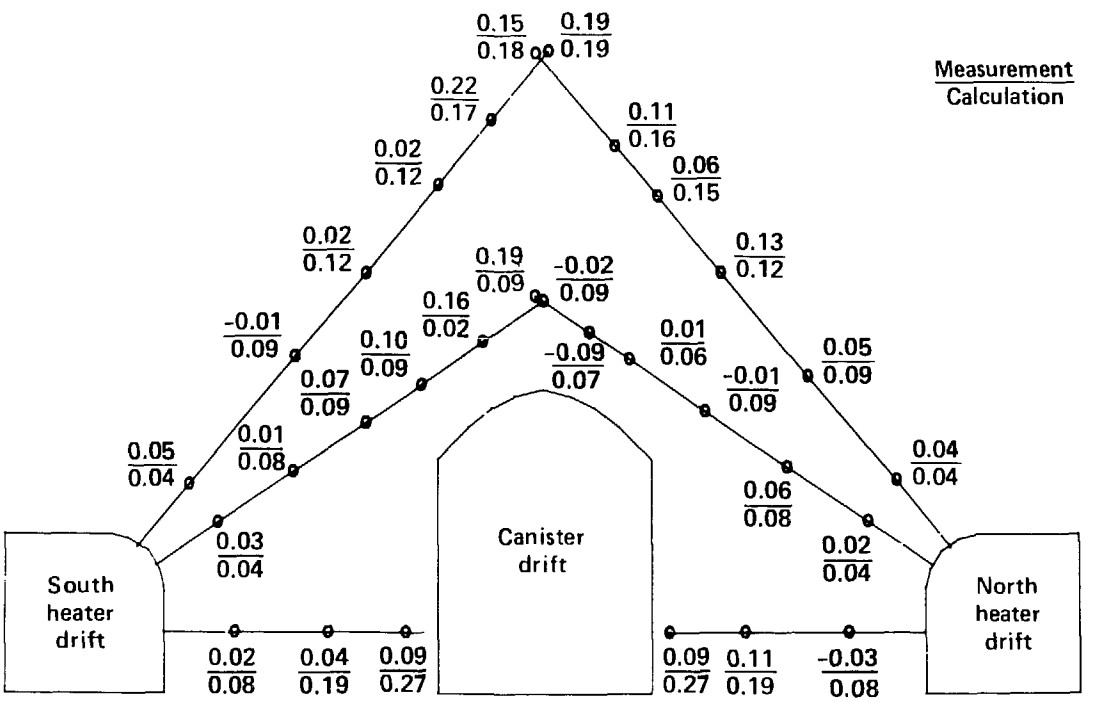

Figure A-9. Results from calculation 3 for Station 2 + 83 at 4.5 YOC.

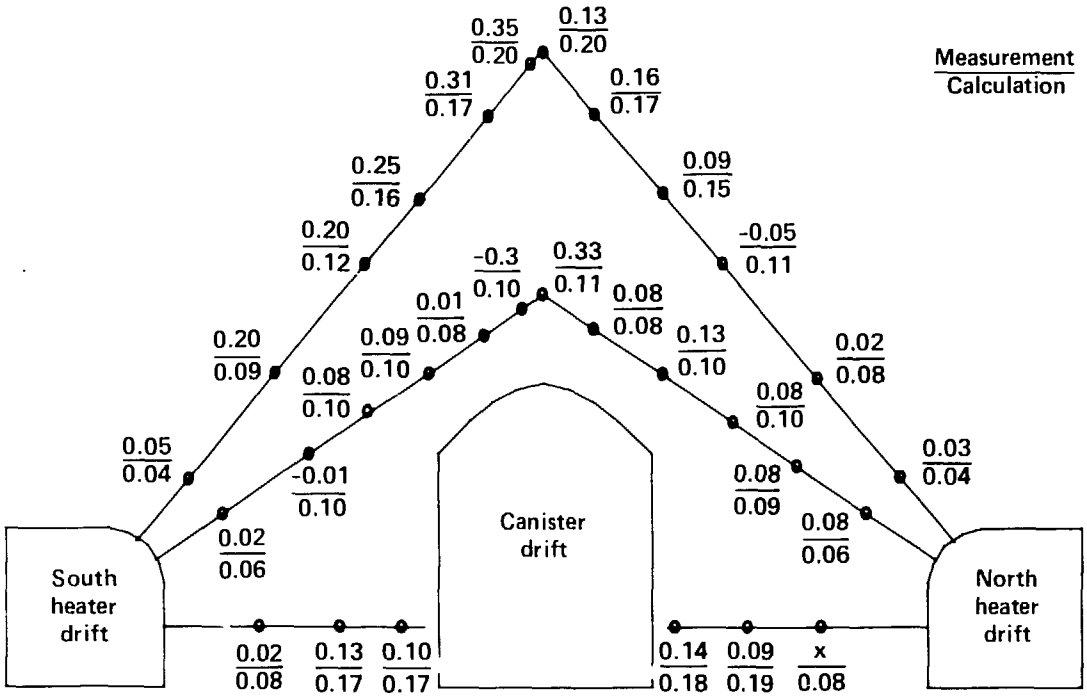

Figure A-10. Results from calculation 1 for Station 3 + 45 at 4.5 YOC.

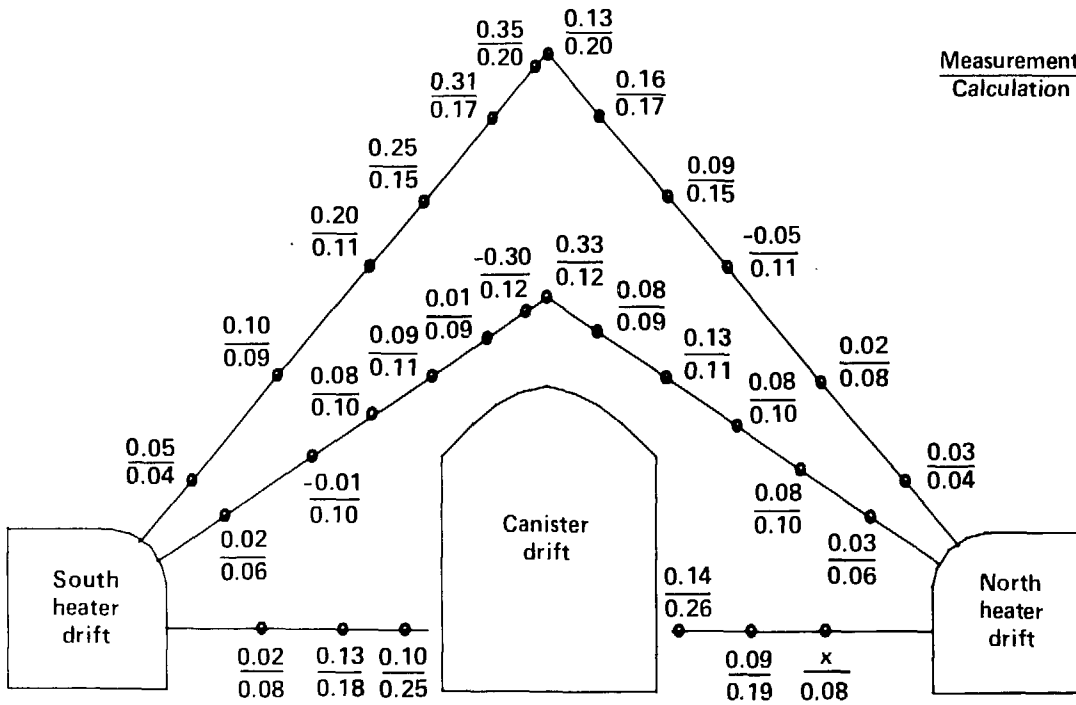

Figure A-11. Results from calculation 2 for Station 3 + 45 at 4.5 YOC.

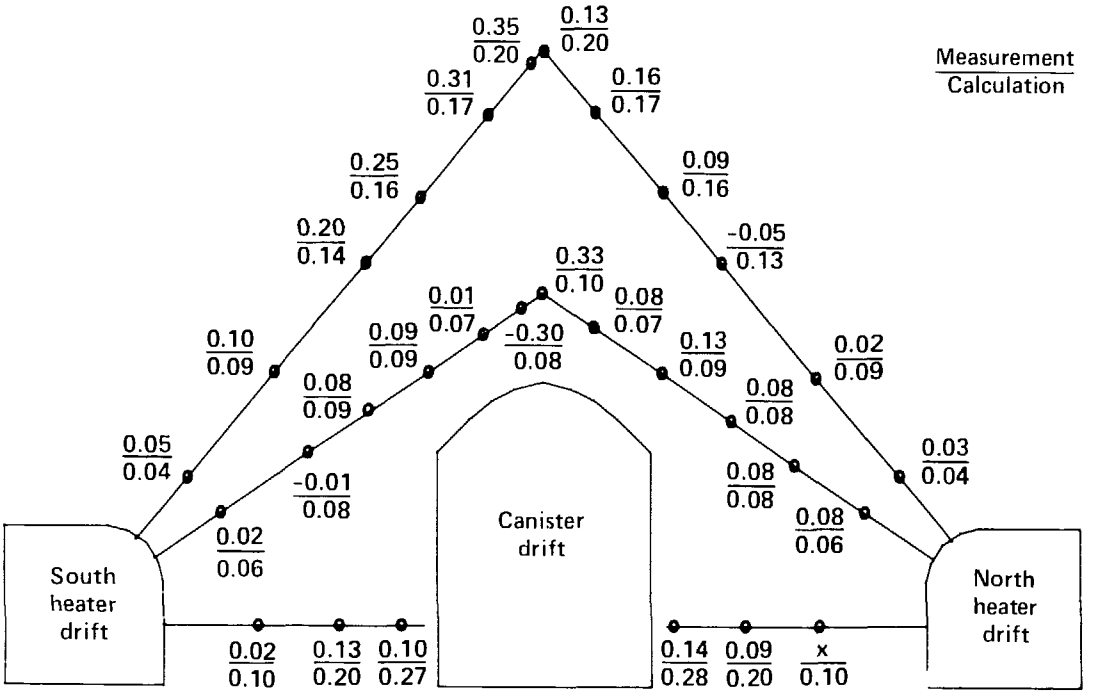

Figure A-12. Results from calculation 3 for Station 3 + 45 at 4.5 YOC.

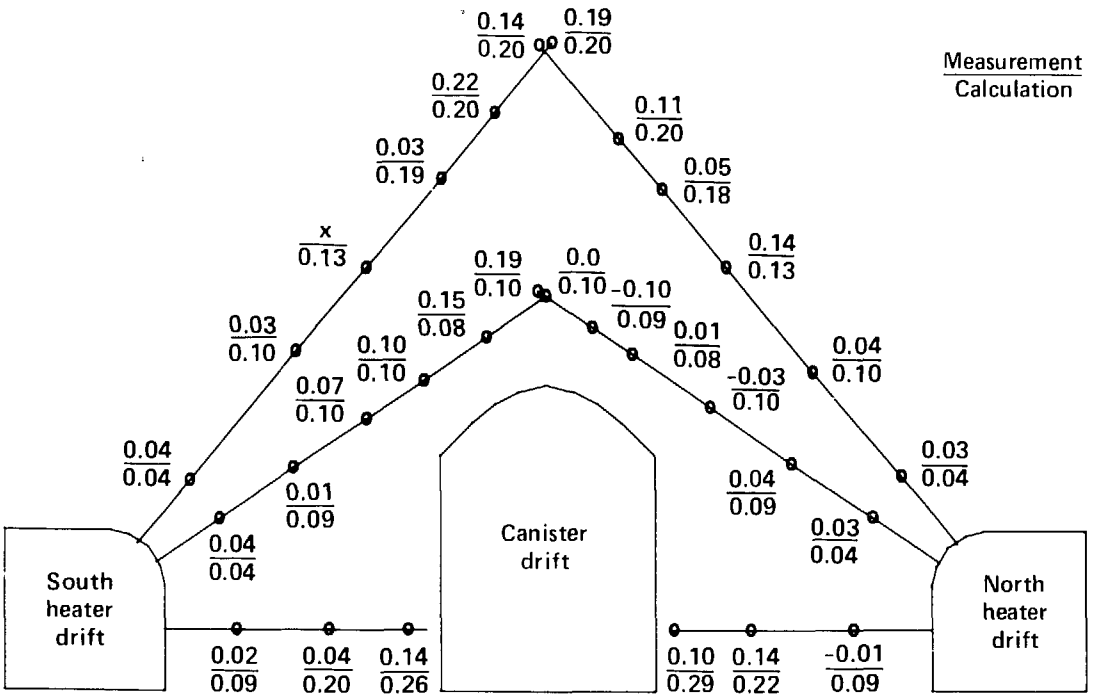

Figure A-13. Results from calculation 1 for Station 2 + 83 at 5.25 YOC.

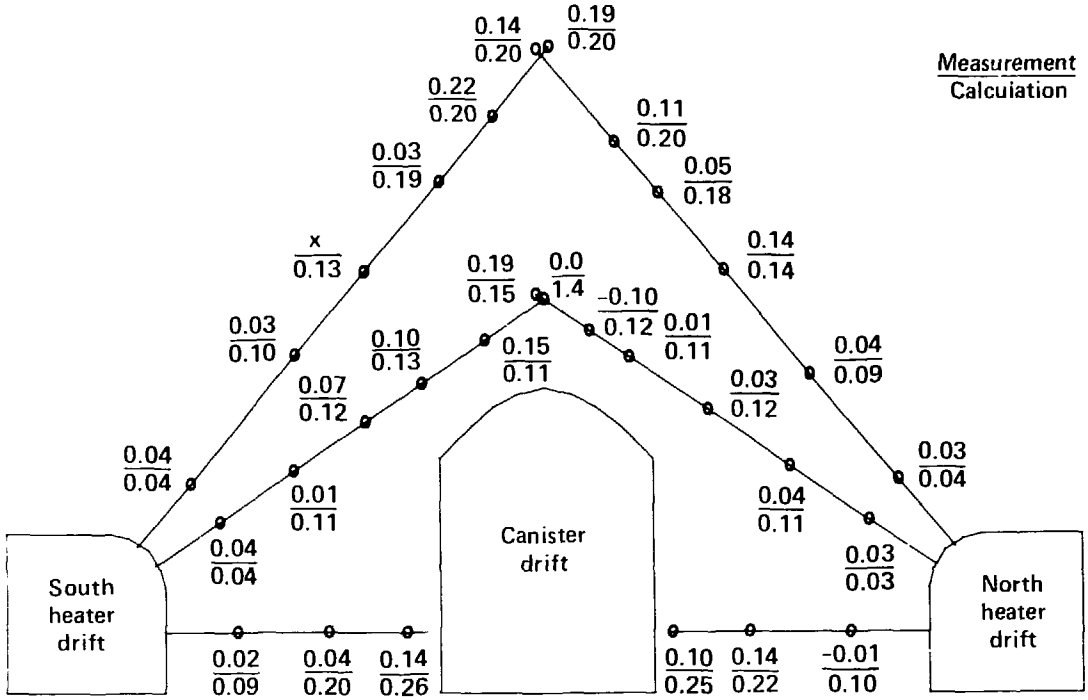

Figure A-14. Results from calculation 2 for Station 2 + 83 at 5.25 YOC.

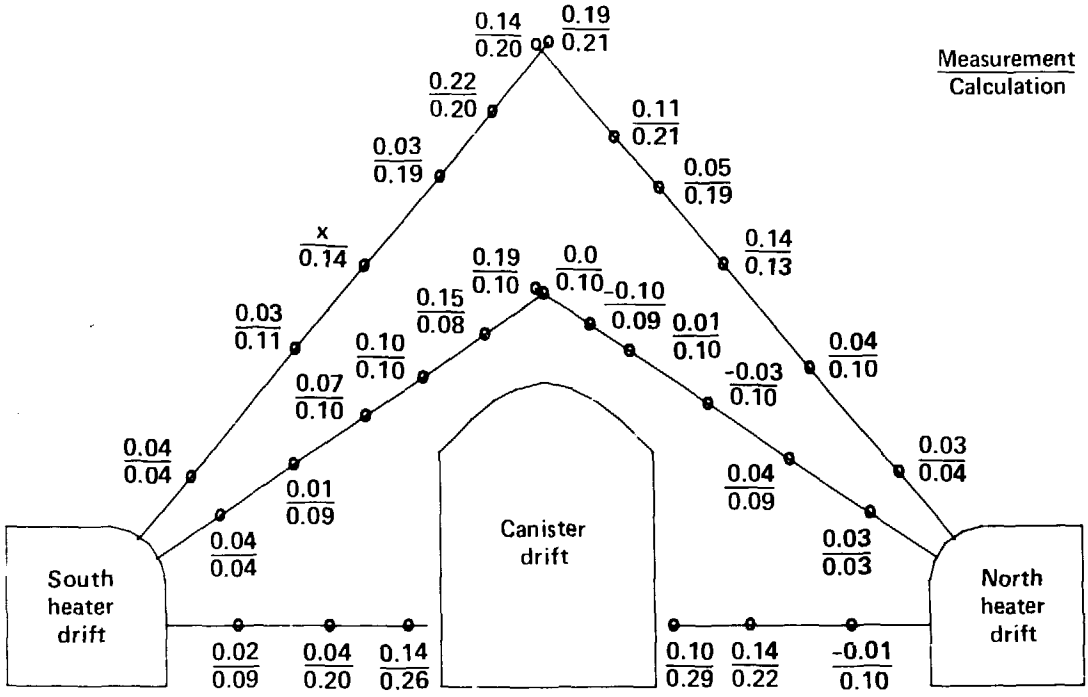

Figure A-15. Results from calculation 3 for Station 2 + 83 at 5.25 YOC.

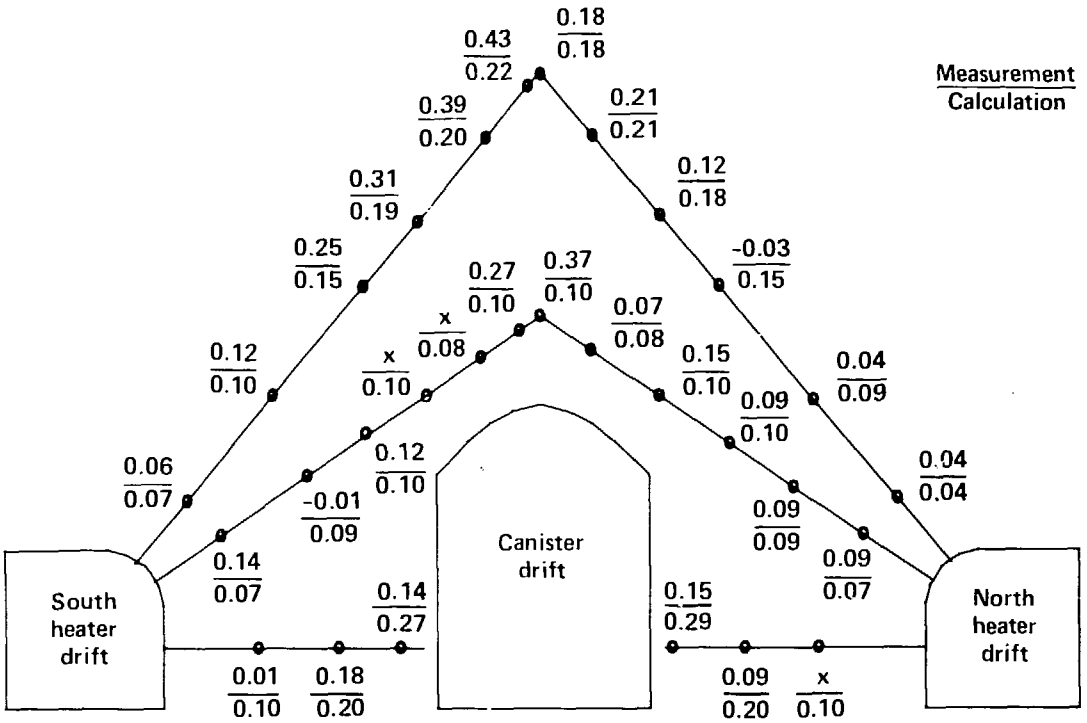

Figure A-16. Results from calculation 1 for Station 3 + 45 at 5.25 YOC.

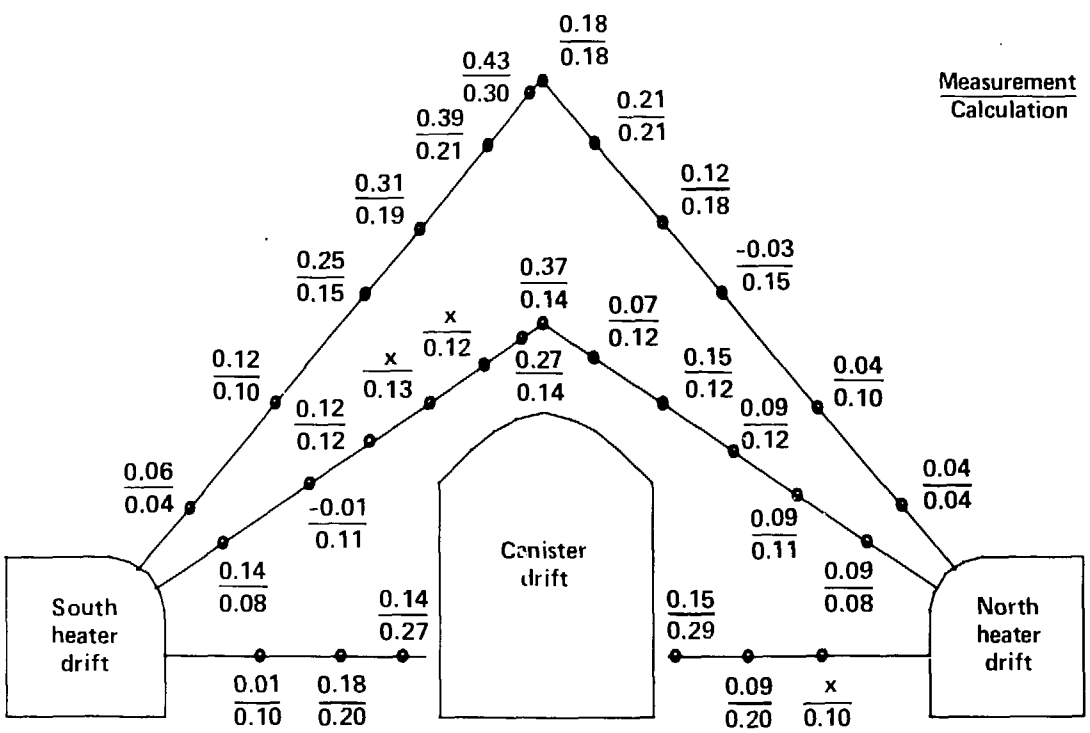

Figure A-17. Results from calculation 2 for Station 3 + 45 at 5.25 YOC.

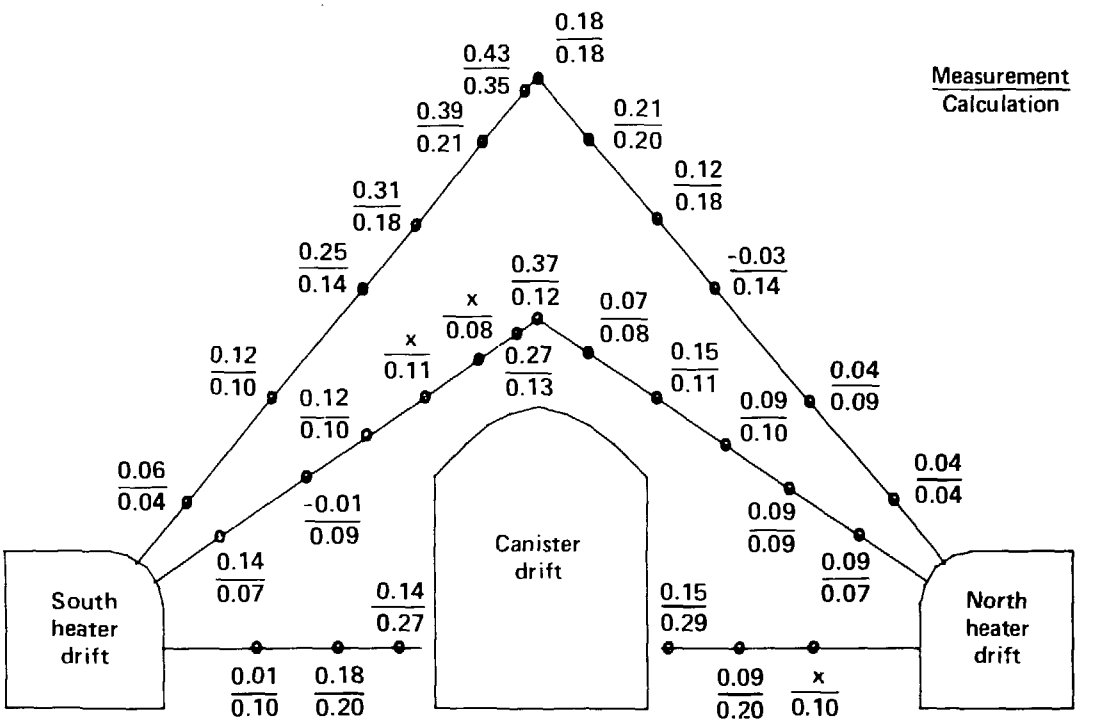

Figure A-18. Results from calculation 3 for Station 3 + 45 at 5.25 YOC.

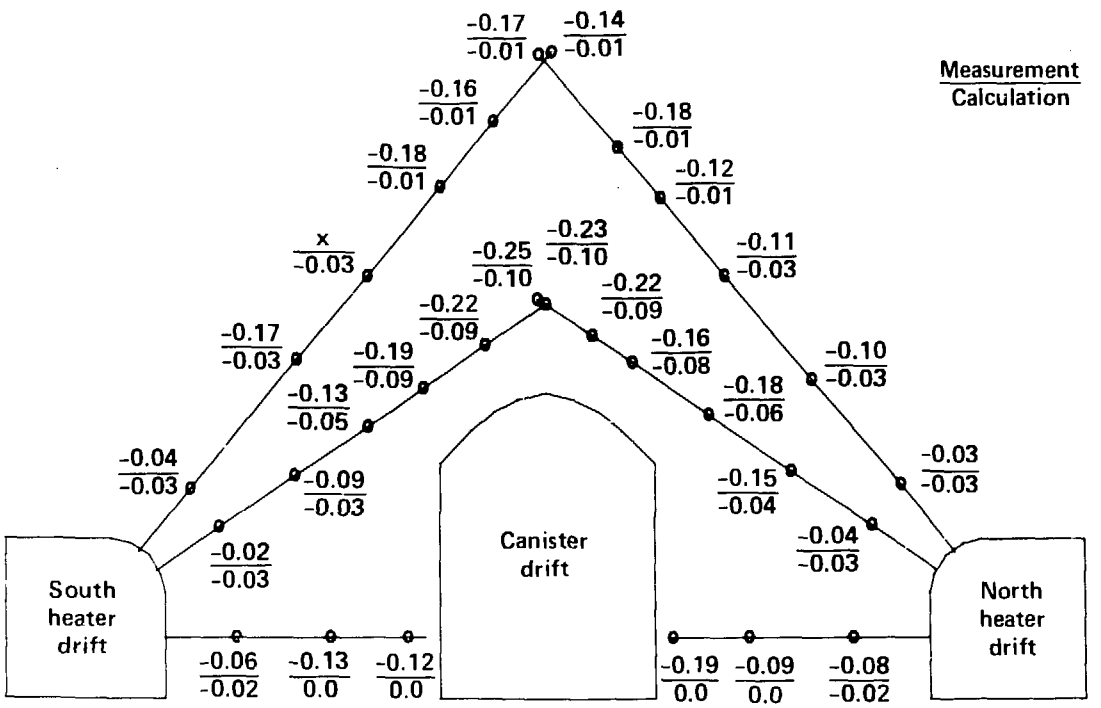

Figure A-19. Results from calculation 1 for Station 2 + 83 at 5.86 YOC.

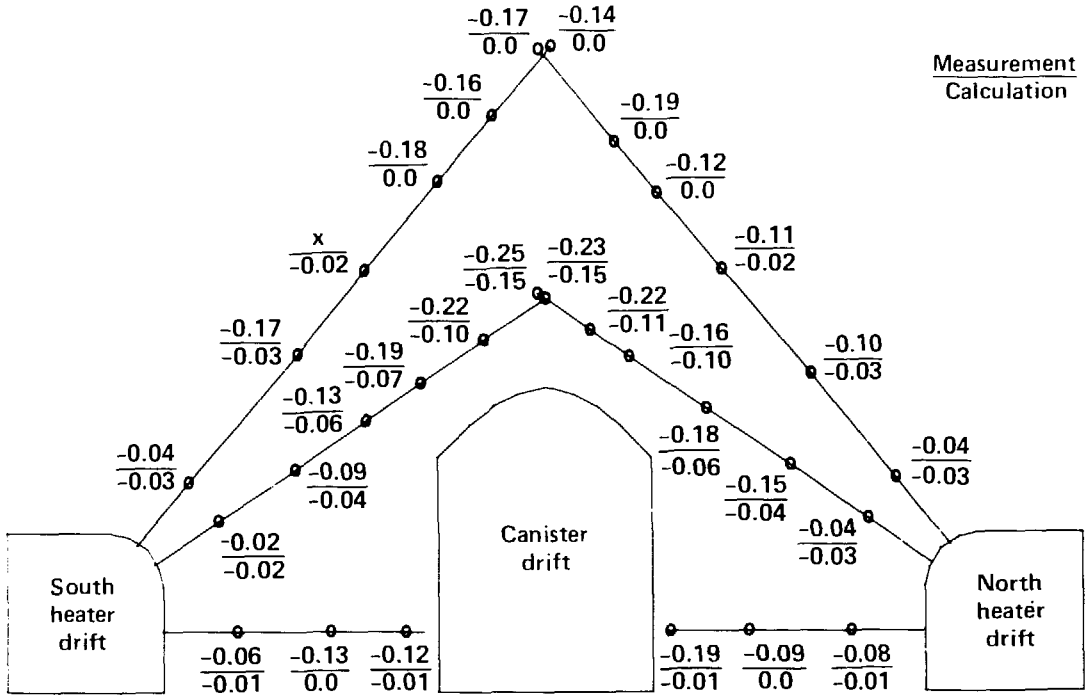

Figure A-20. Results from calculation 2 for Station 2 + 83 at 5.86 YOC.

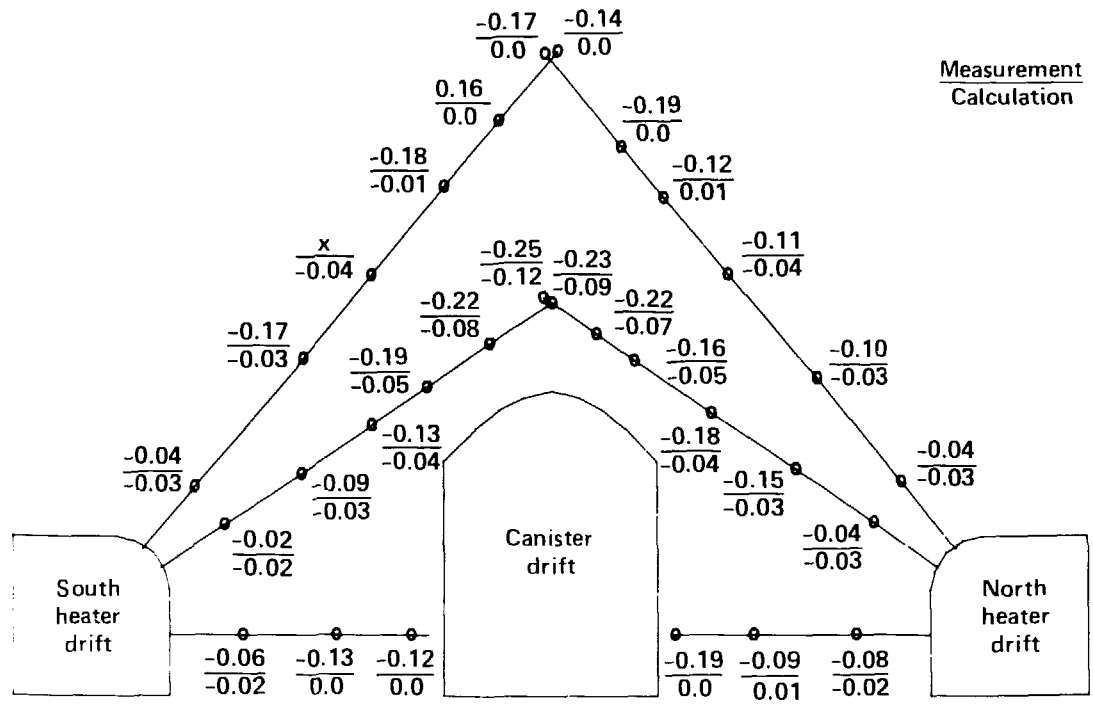

Figure A-21. Results from calculation 3 for Station 2 + 83 at 5.86 YOC.

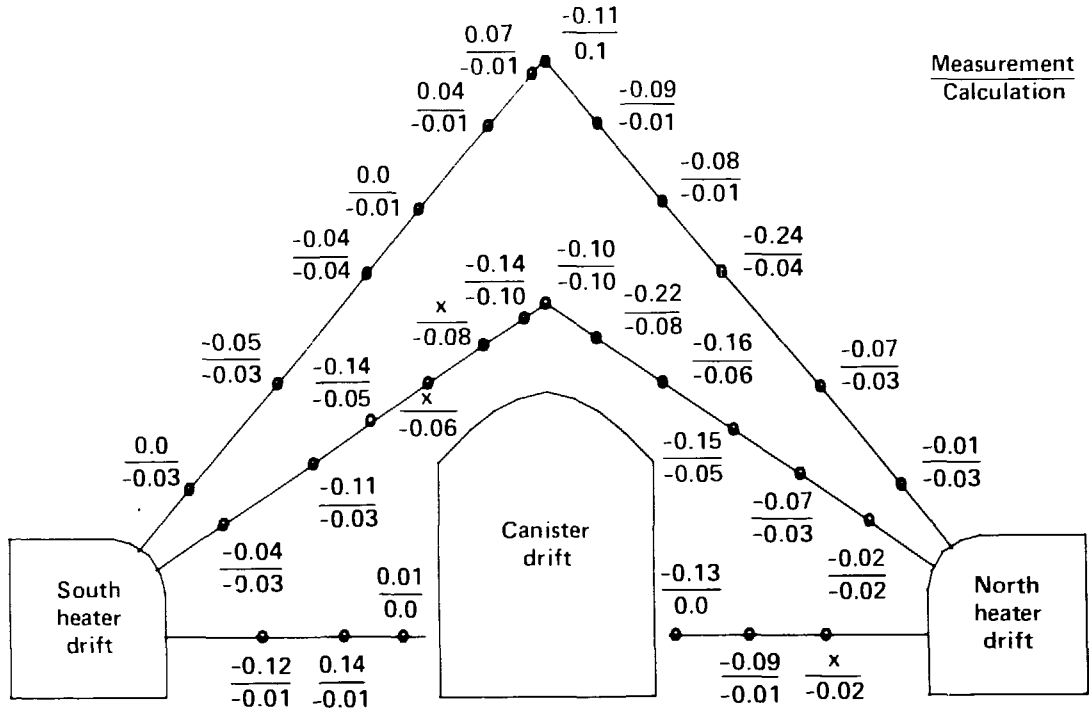

Figure A-22. Results from calculation 1 for Station 3 + 45 at 5.86 YOC.

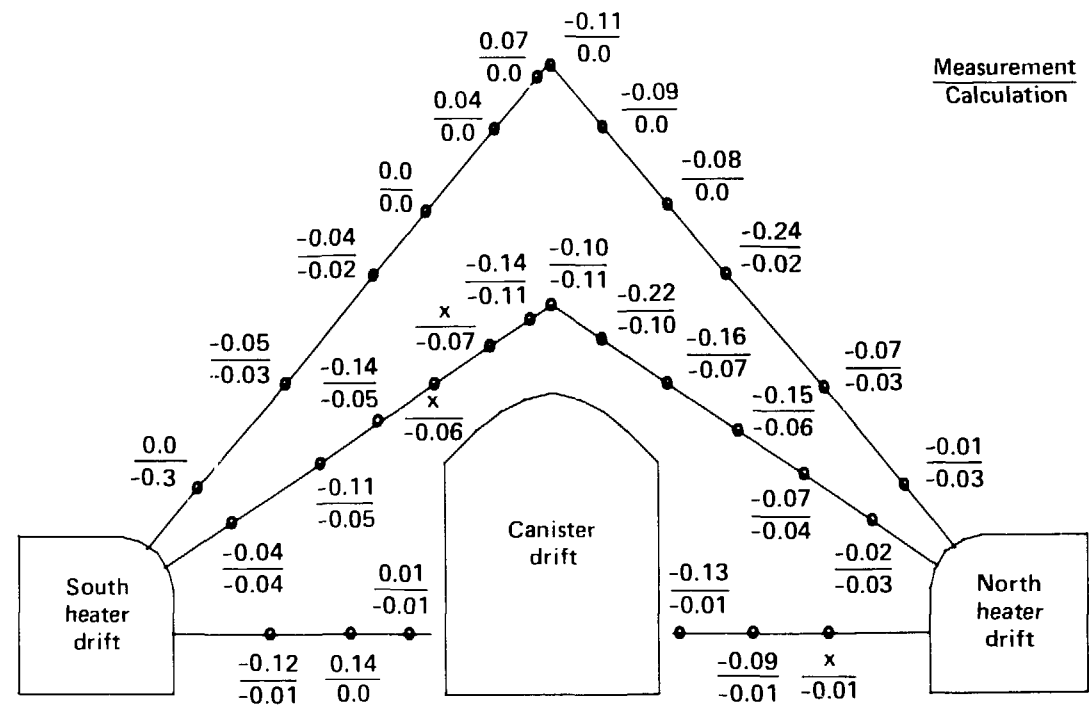

Figure A-23. Results from calculation 2 for Station 3 + 45 at 5.86 YOC.

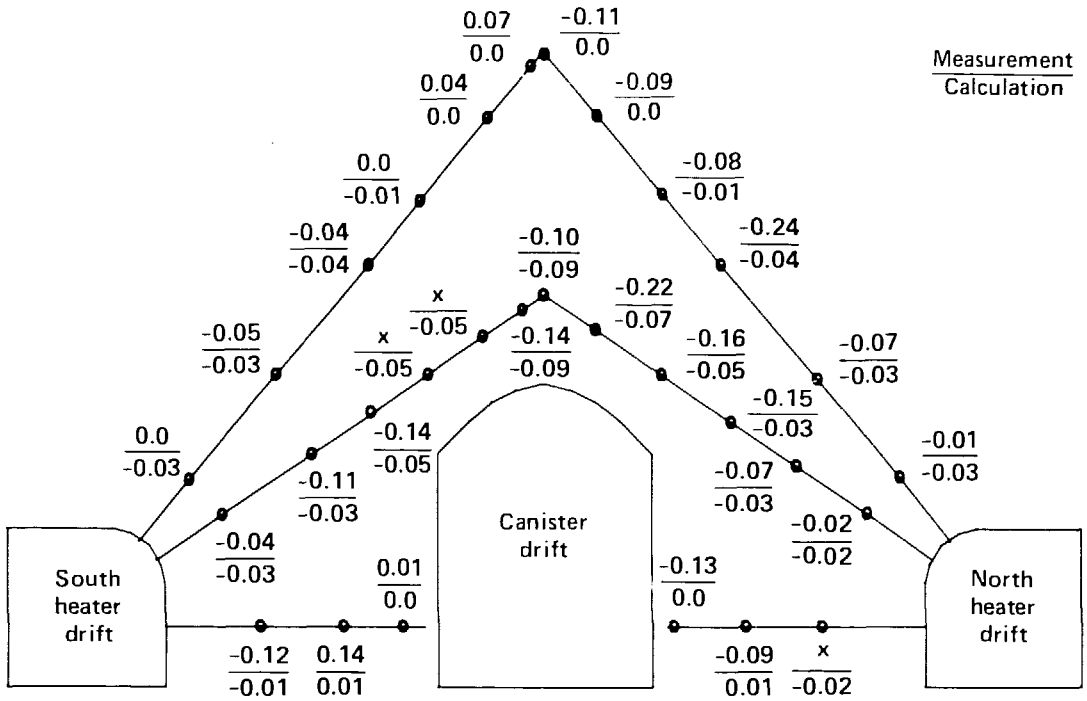

Figure A-24. Results from calculation 3 for Station 3 + 45 at 5.86 YOC.

U. S. Government Printing Office: 1986/10-785-002/44121